Title

Revisiting the Analytical Solutions of Heat Transport in Fractured Reservoirs Using a Generalized Multirate Memory Function

Journal

Water Resources Research, 55(2)

ISSN

0043-1397

Authors

Zhou, Quanlin
Oldenburg, Curtis M
Rutqvist, Jonny

Publication Date

2019-02-01

DOI

10.1029/2018wr024150

Peer reviewed

Revisiting the Analytical Solutions of Heat Transport in Fractured Reservoirs Using a Generalized Multirate Memory Function

Quanlin Zhou[1], Curtis M. Oldenburg[1], and Jonny Rutqvist[1]

[1] Energy Geosciences Division, Lawrence Berkeley National Laboratory, Berkeley, CA, USA

Correspondence to: Q. Zhou, qzhou@lbl.gov

Abstract

Numerous analytical solutions have been developed for modeling thermal perturbations to underground formations caused by deep-well injection of fluids. Each solution has been derived for a specific boundary value problem and a simplified flow network with one set of parallel fractures. In this paper, new generalized solutions $G^*(x,s)$ are developed using (existing) global transfer functions $G_0^*(x,s)$ and a new memory function $g^*(s)$, where x and s are the space and Laplace variable. The memory function represents the solutions of conductive heat exchange between fractures and matrix blocks and between fractured aquifers and unfractured aquitards. The memory function is developed to account for multirate exchange induced by different shapes, sizes, properties, and volumetric fractions of matrix blocks bounded by *multiple sets of orthogonal fractures* with different spacing. The global transfer functions represent the fundamental solutions to convective, convective-conductive, and convective-dispersive heat transport in fractures (or aquifers) without exchange and are available for various (1-D linear, 1-D radial, 2-D dipole, and single-well injection-withdrawal) flow fields. The new solutions with exchange are developed using $G^*(x,s) = B^*(s)G_0^*\{x, s[1+\vartheta g^*(s)]\}$, thereby greatly simplifying solution development in a novel way, where ϑ and $B^*(s)$ are a fracture-matrix scaling factor and the boundary condition function. The new solutions are applied to several example problems, showing that heat transport in fractured aquifers is significantly impacted by (1) thermal dispersion in fractures that is rarely considered, (2) multirate heat exchange with a wide range of size and anisotropy of rectangular matrix blocks, and (3) heat exchange between aquifers and aquitards.

1 Introduction

Thermal perturbations to underground formations can be caused by injecting fluids of different temperature into the deep subsurface or by natural recharge of surface water with sinusoidally time-varying temperature into the shallow subsurface. Relevant applications involving fluid injection may be directly related to energy storage and production, such as for thermal oil recovery (Kuhn & Koch, 1953; Walter, 1957), aquifer thermal energy storage (Andersson et al., 2013; Meyer & Todd, 1973; Nordbotten, 2017; Tsang et al., 1982), and geothermal energy production (Bodvarsson & Eggers, 1972; Gringarten et al., 1975; Harlow & Pracht, 1972), or they may not be energy

related, such as for waste-water disposal, water flooding for secondary oil recovery, and geological CO_2 storage. Relevant applications in the latter include estimating the rate of groundwater recharge using field temperature measurements (Bredehoeft & Papadopulos, 1965; Constantz et al., 2002; Hatch et al., 2006; Silliman et al., 1995; Stallman, 1965; Suzuki, 1960).

Injection-induced thermal perturbations can propagate through deep reservoirs by the processes of convection, conduction, and thermal dispersion. Analytical solutions of the convection equation, the convection-conduction equation, and the convection-dispersion equation are available in the literature for 1-D linear (Carslaw & Jaeger, 1959; Ogata & Banks, 1961), 1-D radial (Carslaw & Jaeger, 1959; Moench & Ogata, 1981; Tang & Babu, 1979), and 2-D dipole (Grove & Beetem, 1971) fluid flow in homogeneous reservoirs, with local thermal equilibrium assumed between the resident and injected fluids and the porous matrix. These fundamental solutions without fracture-matrix and aquifer-aquitard exchange are referred to as global transfer functions $G_0(x,t)$ and $G_0^*(x,s)$, where x and s are the space and Laplace variable, respectively, and t is the time.

When fluid injection occurs in aquifers bounded by overlying and underlying aquitards, the dynamic heat exchange between the aquifers and the aquitards has to be considered. This complexity has led to a large number of analytical solutions developed to account for the coupled local heat exchange and global heat transport in different flow fields and with various boundary conditions (e.g., Avdonin, 1964a, 1964b; Carslaw & Jaeger, 1959; Chen & Reddell, 1983; Kocabas, 2004; Lauwerier, 1955; Li et al., 2010; Noyer, 1977; Rubinshtein, 1960, 1962; Spillette, 1965). The local heat exchange in these solutions has been restricted to semi-infinite or finite aquitards, and the so-called memory function $g^*(s)$ for 1-D conductive heat exchange is either $g^*(s) \propto 1/\sqrt{s}$ for the semi-infinite aquitards or $g^*(s) \propto \coth(\sqrt{s})/\sqrt{s}$ for the finite aquitards with fixed temperature.

For thermal perturbations in fractured reservoirs, analytical solutions have been developed by exploiting the analogy between fractures and aquifers and between matrix blocks and aquitards for single (or parallel) fractures and semi-infinite (or finite) slab-like matrix blocks (Abbasi et al., 2017; Ascencio et al., 2014; Bodvarsson, 1969; Bodvarsson & Tsang, 1982; Gringarten et al., 1975; Jung & Pruess, 2012; Kocabas, 2005). This configuration of nonoverlapping parallel fractures and matrix blocks is oversimplified because it neglects the complex networks of natural fractures and the multitude of matrix blocks with different shapes and sizes. The memory function for heat exchange between parallel fractures and finite slabs is $g^*(s) \propto \tanh(\sqrt{s})/\sqrt{s}$. Analytical solutions based on the dual-continuum concept are available for pressure propagation (Moench, 1984) and solute transport (Moench, 1995) in fractured reservoirs but only for the exact exchanges between fractures and isotropic matrix blocks (slab, sphere, and cylinder).

The continuum-based numerical models with overlapping fracture and matrix continua, such as the dual-porosity model (Barenblatt et al., 1960; Warren & Root, 1963) and the multiple-interacting-continuum model (Pruess & Narasimhan, 1985), are not accurate in capturing the dynamic, local heat exchange at fracture-matrix interfaces (e.g., Guan et al., 2008; Lim & Aziz, 1995; Zhou et al., 2006). Discrete fracture-matrix (DFM) models (e.g., Sandve et al., 2012) employ fine discretization of both fractures and the matrix blocks. However, the accuracy of the DFM models depends on the approximation of fracture-matrix heat exchange and the resolution of discretization of each of many matrix blocks. In summary, the weakness of existing analytical solutions arises either from the oversimplified geometry of (nonoverlapping) parallel fractures and slab-like matrix blocks or from the isotropic geometry of matrix blocks in dual-continuum analytical solutions. The gap in numerical models is the limited accuracy of the dual-porosity and multiple-interacting-continuum models or the large number of grid blocks (nodes) needed to resolve the large number of fractures and matrix blocks at the reservoir scale.

In this paper, we develop a suite of analytical solutions, $G^*(x,s)$, of heat transport in fractured reservoirs bounded by aquitards using the concept of transfer function for linear transport systems (Danckwerts, 1953; Sardin et al., 1991; Villermaux, 1987). A representative elementary volume (REV) of the fractured reservoir is conceptualized to contain *multiple rectangular matrix blocks* with different sizes, aspect ratios, properties, and volume fractions that are bounded by *multiple well-mixed orthogonal fractures*. A generalized multirate memory function, $g^*(s)$, is developed using the diffusive flux equation (Zhou, Oldenburg, Rutqvist, & Birkholzer, 2017; Zhou, Oldenburg, Spangler, & Birkholzer, 2017) to account for multirate conductive heat exchange between fractures and matrix blocks per unit matrix volume of a REV. The suite of analytical solutions is developed in the form: $G^*(x,s) = B^*(s)G_0^*\{x, s[1+\vartheta g^*(s)]\}$ by plugging the memory function into existing global transfer functions $G_0^*(x,s)$ to model global heat convective, convective-conductive, and convective-dispersive transport in fractured reservoirs with different flow fields, where ϑ and $B^*(s)$ are a fracture-matrix scaling factor and the boundary condition function, respectively.

We apply the developed dual-continuum-based analytical solutions to several benchmark problems under different flow conditions. Some of the benchmark problems contain a collection of multiple sets of orthogonal fractures and matrix blocks of multiple shapes (1-D slabs, 2-D rectangles, and 3-D rectangular parallelepipeds) and sizes. The solutions to these benchmark problems can be used to compare DFM modeling with orthogonal fracture networks of different fracture density and spacing. These benchmark problems bridge the gap between representing natural fracture networks and matrix blocks by existing analytical solutions and DFM modeling.

2 Mathematical Modeling of Multirate Heat Transport in Fractured Reservoirs

In this study, we are interested in heat transport in fractured reservoirs that may be overlain and underlain by aquitards (see Figure 1). The REV of the fractured medium crosses the entire thickness of the reservoir and may contain a number of fractures of different finite lengths and a number of matrix blocks that may have different shapes, sizes, properties, and volume fractions. To derive analytical solutions, we introduce the following assumptions: (1) the fluid flow is 1-D linear, 1-D radial, or 2-D dipole through the connected fracture network, (2) the thicknesses of the fractured reservoir and overlying and underlying aquitards are constant, (3) the volume fraction of the fracture continuum is constant at the REV scale of the fractured medium, (4) fracture temperature within a REV is assumed uniform, that is, fracture fluid is well mixed, (5) the fractured reservoir is homogeneous and isotropic at the REV scale, and (6) only horizontal thermal conduction in the fracture continuum and vertical thermal conduction in the homogeneous aquitards are considered.

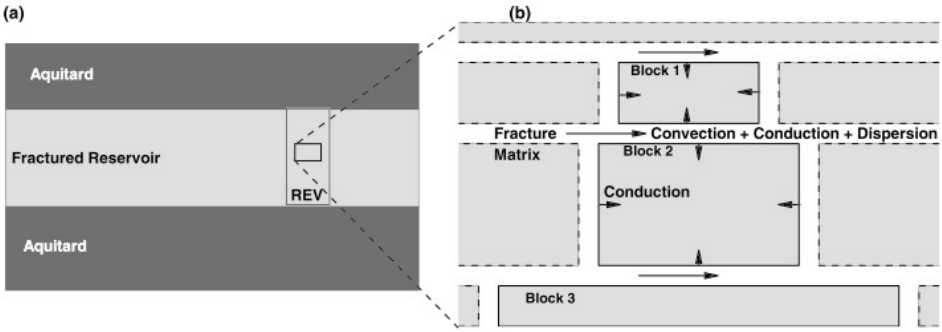

Figure 1. (a) A fractured reservoir overlain and underlain by aquitards with a representative elementary volume (REV) spanning the entire reservoir thickness and (b) a portion of the REV consisting of multiple fractures and matrix blocks of different shapes and sizes, as well as heat convection-conduction-dispersion in fractures coupled with heat conduction in matrix blocks.

2.1 Thermal Dispersion in Fracture Networks

Heat transport includes two fundamental pore-scale processes: conduction and convection. For heat conduction in porous media, the bulk heat conductivity is often used to account for the collective behavior of heat conduction through fluids in pores and through solid grains. For heat convection through the pore space, the (macroscopic) convection with mean pore velocity and thermal dispersion may be used in the same way that solute advective and dispersive transport at the macroscopic level are considered; that is, thermal dispersion is caused by variations in pore velocity from the mean velocity. The coefficient of thermal dispersion has been measured in laboratory experiments (e.g., Green et al., 1964; Metzger et al., 2004; Rau et al., 2012; Yagi et al., 1960) or calculated from numerical experiments (e.g., Kuwahara & Nakayama, 1999; Saada et al., 2006; Vafai & Tien, 1981). It has been found that the ratio of the effective to intrinsic thermal conductivity is a function of the particle-based Peclet number (i.e., product of the Reynolds number and the Prandtl number), as critically reviewed by Ozgumus et al. (2013). In subsurface hydrology, thermal dispersion has only been considered in heat-transport modeling by a few

researchers (e.g., Kocabas, 2004; Molina-Giraldo et al., 2011; Sauty et al., 1982).

Unlike for ground-source building-scale heat-pump problems with small groundwater flow velocity (Molina-Giraldo et al., 2011), thermal dispersion may be important in unfractured reservoirs near large-volume injection wells where fluid velocity and the Peclet number are large. For fractured reservoirs, both fluid velocity and the Peclet number are very large near injection wells, leading to a large radial extent of high thermal dispersion. For example, the fluid velocity varies from 0.1 m/s at a radius of 1 m to 10^{-4} m/s at a radius of 1,000 m for a fractured reservoir with a thickness of 10 m, a volume fraction of the fracture network of 0.01, and a typical injection rate of 2×10^6 m^3/year. The actual radial extent of thermal perturbations is, however, significantly smaller than the acting radius of thermal dispersion because of limited travel distance of convective-dispersive heat transport due to retardation by strong fracture-matrix heat exchange.

Following the many studies on thermal dispersion, we can write the effective thermal conductivity tensor (λ_e) as the summation of the intrinsic thermal conductivity (λ) of fluid and grains and the dispersion-induced thermal conductivity (λ_d):

$$\lambda_e = \lambda + \lambda_d\left(P_e^{'}\right), \quad (1a)$$

where λ_d is a function of the Peclet number ($P_e^{'}$) with respect to the length scale of velocity variations (e.g., grain size). The two principal components of the effective thermal conductivity tensor can be written as follows:

$$\lambda_{eL} = \lambda_L + \lambda_{dL}\left(P_e^{'}\right) = \lambda_L + \alpha_L u \rho_w c_w, \quad (1b)$$

and

$$\lambda_{eT} = \lambda_T + \lambda_{dT}\left(P_e^{'}\right) = \lambda_T + \alpha_T u \rho_w c_w, \quad (1c)$$

where α is the thermal dispersivity, u is the longitudinal fluid velocity, ρ_w is the density of water, c_w is the specific heat of water, and subscripts L and T denote the longitudinal and transverse values for thermal conductivities and thermal dispersivity, respectively. For 1-D linear fluid and heat flow, $\lambda_{eL}(=\lambda_L + \alpha_L u \rho_w c_w)$ can be used easily as it is constant because u and $P_e^{'}$ are constant. For 1-D radially diverging flow, both u and $P_e^{'}$ decrease with the radial distance away from the injection well, leading to λ_{eL} decreasing asymptotically to the intrinsic thermal conductivity λ_L. It is often assumed in analytical heat-transport modeling that $\lambda_{eL}(=\lambda_L)$ is constant in the case of low u and $P_e^{'}$, or $\lambda_{eL}(=\alpha_L u \rho_w c_w)$ is radius dependent in the case of a high injection rate. In what follows, we omit subscript L for 1-D linear or radial flow.

2.2 Heat Transport Equations for Fracture Continuum

The governing equation of heat transport in the fracture continuum per unit volume of REV of the fractured medium under a steady state fluid flow can be written (Bear, 1972) as follows:

$$\frac{\partial}{\partial t}\left(\theta_f \rho_f c_f T_f\right) = \theta_f\left\{\nabla\cdot\left(\boldsymbol{\lambda}_{ef}\cdot\nabla T_f\right) - \rho_w c_w \boldsymbol{q}_f\cdot\nabla T_f\right\} - \Gamma_{fm} - \Gamma_{aa}, \quad (2a)$$

where θ_f is the REV-scale volume fraction of the fracture continuum in the fractured medium, $\rho_f c_f$ (=$(1-\phi_f)\rho_g c_g + \phi_f \rho_w c_w$) is the volumetric heat capacity of the fracture continuum, $\rho_w c_w$ and $\rho_g c_g$ are the volumetric heat capacity of water and grains respectively, ϕ_f is the intrinsic porosity of fractures, λ_{ef} is the effective thermal conductivity tensor of the fractures, including intrinsic and dispersion-induced thermal conductivity, q_f (=$\phi_f u_f$) is the vector of Darcy's velocity in the fractures, u_f is the vector of mean pore-water velocity in the fractures, T_f is the temperature of fractures, Γ_{fm} is the heat sink (positive) from fractures to matrix blocks (or the heat source from matrix blocks to fractures) per unit volume of REV of the fractured media, Γ_{aa} is the heat sink (positive) from the aquifer to aquitards (or the heat source from aquitards to the aquifer) per unit volume of REV of the fractured media, ∇ is the gradient operator, and $\nabla\cdot$ is the divergence operator.

The heat source/sink term Γ_{fm} can be written using convolution (Carrera et al., 1998; Dentz & Berkowitz, 2003):

$$\Gamma_{fm} = \theta_m \rho_w c_w \int_0^t g\left(t'\right)\frac{\partial T_f\left(t-t'\right)}{\partial t}\,\mathrm{d}t', \quad (2b)$$

where θ_m (=$1-\theta_f$) is the REV-scale volume fraction of matrix blocks in the fractured media, $g(t)$ (T^{-1}) is the normalized conductive heat flux at the fracture-matrix interfaces per unit volume of the rock matrix (in the REV of fractured media) per unit (constant) temperature change at fractures. The normalization is conducted by scaling the fracture-matrix conductive heat flux by the volumetric heat capacity, $\rho_w c_w$, of water. This normalized diffusive flux is often referred to as the memory function in the community of solute-transport modeling (Carrera et al., 1998; Dentz & Berkowitz, 2003; Haggerty et al., 2000).

Similarly, we can write the heat source/sink term Γ_{aa} for a unit volume of REV of the fractured medium by

$$\Gamma_{aa} = \rho_w c_w \int_0^t g_{aa}\left(t'\right)\frac{\partial T_f\left(t-t'\right)}{\partial t}\,\mathrm{d}t', \quad (2c)$$

where g_{aa} is the memory function for the normalized heat flux through the aquifer-aquitard interfaces. In what follows, we will omit Γ_{aa}, unless mentioned otherwise.

Combining equations 2a and 2b leads to the following heat transport equation, with constant fluid and rock properties assumed:

$$\nabla\cdot\left(\boldsymbol{D}_{ef}\cdot\nabla T_f\right)-\frac{1}{R_f}\boldsymbol{q}_f\cdot\nabla T_f-\left[\frac{\partial T_f}{\partial t}+\vartheta\int_0^t g\left(t'\right)\frac{\partial T_f\left(t-t'\right)}{\partial t}\mathrm{d}t'\right]=0, \quad (3a)$$

with

$$R_f=\rho_f c_f/\rho_w c_w,\ \boldsymbol{D}_{ef}=\boldsymbol{\lambda}_{ef}/\rho_f c_f,\ \vartheta=\theta_m/\theta_f R_f, \quad (3b)$$

where R_f (≤1) is the enhancement factor (equivalent to the retardation factor in solute transport), ϑ is the REV-scale fracture-matrix scaling factor related to the REV-scale volume fractions of the fracture and matrix continua and the fracture enhancement factor, and D_{ef} is the effective thermal diffusivity tensor for fractures. The longitudinal component of D_{ef} is

$$D_{ef}=D_f+D_{df}=D_f+\alpha_L u/R_f, \quad (3c)$$

where D_f and D_{df} are the longitudinal intrinsic and dispersion-induced thermal diffusivity for fractures, respectively. Note that for solute transport D_e is called the coefficient of hydrodynamic dispersion, D is the coefficient of molecular diffusion, and D_d is the coefficient of mechanical dispersion (Bear, 1972).

Taking the Laplace transform of equation 3a leads to the heat transport equation in the Laplace domain:

$$\mathscr{L}\left[\mathscr{F}\left(T_f\right)\right]-\left[1+\vartheta g^*(s)\right]sT_f^*=0, \quad (4)$$

where $\mathscr{F}\left(T_f\right)$ denotes the first two terms (i.e., the conduction-dispersion term and the convection term) in equation 3a, $\mathscr{L}$ is the operator for Laplace transform, $T_f^*(s)$ is the Laplace transform of $T_f(t)$, $g^*(s)$ is the Laplace transform of $g(t)$, and s is the Laplace variable with respect to real time t. Equation 4 is a second-order ordinary differential equation for $T_f^*(s)$.

The general heat transport equations, equations 3a and 4, can be rewritten for specific flow fields and different forms of effective thermal diffusivity (see Appendix A).

2.3 Multirate Heat Conduction in Matrix and Aquitards

As shown in Figure 1, the fractured reservoir of interest may contain thousands to millions of discrete fractures with a varying degree of connectivity (Hyman et al., 2015) and finite matrix blocks with irregular shapes and different sizes. Convection and conduction/dispersion prevail within each connected fracture with variable aperture (Detwiler et al., 2000), mixing occurs at the intersections of connected fractures (Park et al., 2001), and diffusion is dominant within matrix blocks (Neretnieks, 1980). Within a REV of the fractured medium, there are a number of matrix blocks with different shapes, sizes, properties, and volume fractions, while the temperature of fractures can be assumed uniform because fracture fluid is well mixed.

We are interested in the memory function $g(t)$ for the (normalized) transient heat flux through fracture-matrix interfaces per unit volume of the rock matrix per unit temperature change at fractures. The REV of fractured media may contain K classes of matrix blocks of different shapes and different sizes that have a minimum fracture half-spacing l^k (k = 1, 2, … , K), a fraction of matrix volume w_m^k, an intrinsic porosity ϕ_m^k, and an intrinsic thermal diffusivity D_m^k. The normalized heat flux between the matrix blocks and fractures per unit volume of the rock matrix is written as follows:

$$g(t) = \sum_{k=1}^{K} w_m^k R_m^k f^k(t) = \sum_{k=1}^{K} \left[w_m^k R_m^k \frac{D_m^k}{\left(l^k\right)^2} \right] f_d^k\left(t_d^k\right), \quad (5a)$$

with

$$R_m^k = \left(\rho_m c_m\right)^k / \rho_w c_w, \left(\rho_m c_m\right)^k = \left(1-\phi_m^k\right)\rho_g c_g + \phi_m^k \rho_w c_w, t_d^k = D_m^k t / \left(l^k\right)^2, \quad (5b)$$

where R_m^k is the enhancement factor of matrix block k, $(\rho_m c_m)^k$ is the volumetric heat capacity of matrix block k, $f^k(t)$ (T^{-1}) and $f_d^k\left(t_d^k\right)$ (−) are the normalized and dimensionless normalized heat flux for a unit change in fracture temperature and a uniform initial matrix temperature, respectively, and t_d^k is the dimensionless time. The normalization is conducted using $\theta_m \rho_w c_w$ as shown in equation 2b.

Note that the memory function defined in equation 5a is only related to the properties of intra-REV matrix blocks and the dimensionless transient heat flux in each matrix block. The fracture-matrix conductive heat flux per unit volume of fractured media is represented by $\theta_m \rho_w c_w g(t)$. In this way, we focus $g(t)$ on the intra-REV matrix properties and dynamics that are separated from the REV-scale scaling factor ϑ. This is slightly different from the memory function $\varphi(t)$ used by Dentz and Berkowitz (2003) that relates the mobile and immobile concentrations by a convolution in time, but with $\vartheta g^*(s) = \varphi^*(s)$. Our memory function is also different from that defined by Haggerty et al. (2000) that may be physically interpreted as the capacity coefficient multiplied by the residence time distribution in the immobile domain, given a Dirac pulse at the surface. The memory function defined by Carrera et al. (1998) is the same as our dimensionless diffusive flux $f_d^k\left(t_d^k\right)$, with the geometric and rock properties of the matrix blocks considered separately. It is of interest to note that $\vartheta g^*(s) = \frac{\theta_m R_m}{\theta_f R_f} g'^*(s) = \varphi^*(s)$ for matrix blocks of identical R_m; the memory function defined here for heat transport is of the same form as that for solute transport, with (R_f, R_m) as the enhancement factors for heat transport but as the retardation factors for solute transport. We include R_m^k inside the memory function to account for multirate heat conduction for matrix blocks of different geometric and rock properties. Without $\rho_w c_w$, equation 5a is also applicable for solute transport and pressure propagation that can consider the intra-REV heterogeneity of matrix blocks.

Indeed, equation 5a is also applicable to the memory function $g_{aa}(t)$, with the two matrix blocks ($K = 2$) as the overlying and underlying aquitards that may have different properties and sizes (finite or semi-infinite). $g_{aa}(t)$ can be written as follows:

$$g_{aa}(t) = \sum_{k=1}^{2} \frac{B_a^k}{B_f} R_m^k f^k(t) = \sum_{k=1}^{K} \left[\frac{B_a^k}{B_f} R_m^k \frac{D_m^k}{\left(l^k\right)^2} \right] f_d^k\left(t_d^k\right), \quad (5c)$$

where B_f is the thickness of the reservoir, B_a^k is the half-thickness of aquitard k, and f_d^k can have a functional form different from slab-like matrix blocks with a no-flow condition in the center of the aquitards.

The average matrix temperature, $T_m^{av}(t)$, in the REV can be written (Zhou, Oldenburg, Rutqvist, & Birkholzer, 2017; Zhou, Oldenburg, Spangler, & Birkholzer, 2017) as follows:

$$T_m^{av}(t) = \sum_{k=1}^{K} w_m^k \frac{D_m^k}{\left(l^k\right)^2} M_d^k\left(t_d^k\right), \quad (6a)$$

with

$$M_d^k\left(t_d^k\right) = \int_0^{t_d^k} f_d^k\left(t_d'\right) dt_d'. \quad (6b)$$

where M_d^k is the dimensionless cumulative diffusive flux or average temperature for matrix block k in response to unit temperature change in surrounding fractures.

For a single (homogeneous and isotropic) matrix block, the governing equation for heat conduction, with fluid velocity assumed to be negligible, can be written as follows:

$$\frac{\partial}{\partial t}\left(\rho_m c_m T_m\right) = \nabla \cdot \left(\lambda_m \nabla T_m\right), \quad (7)$$

where λ_m is the intrinsic thermal conductivity of the matrix and T_m is the temperature of the matrix. Equation 7 can also be rewritten as follows:

$$\frac{\partial T_m}{\partial t} = D_m \nabla^2 T_m, \quad (8)$$

where D_m ($=\lambda_m/\rho_m c_m$) is the thermal diffusivity of the matrix. Equation 8 has been solved for a matrix block of regular shape (cylinder, sphere, slab, rectangle, and rectangular parallelepiped) with a unit temperature change at its boundary (Carslaw & Jaeger, 1959). In this study, we do not solve equation 8 but directly use the diffusive flux equation (Zhou, Oldenburg, Rutqvist, & Birkholzer, 2017; Zhou, Oldenburg, Spangler, & Birkholzer, 2017) to calculate $f_d^k\left(t_d^k\right)$ and $g(t)$.

3 Analytical Solutions of Multirate Heat Transport in Fractured Reservoirs

In this section, we present a suite of semianalytical solutions to multirate heat transport in fractured reservoirs. These solutions are obtained using the

concept of transfer function for linear transport systems (Danckwerts, 1953; Sardin et al., 1991; Villermaux, 1987). The fracture network is a linear system for global heat transport, and each matrix block is a linear system for local fracture-matrix exchange. Therefore, we use global transfer functions, $G_0(x, t)$, and their Laplace transforms, $G_0^*(x, s)$, to represent global heat convective-conductive-dispersive transport in the fracture network without fracture-matrix exchange. These $G_0^*(x, s)$, available in the literature for different flow fields, are listed in section 3.3. We also use a local memory function, $g(t)$, and its Laplace transform, $g^*(s)$, to represent the conductive heat flux through fracture-matrix interfaces per unit temperature change in fractures. A new memory function, $g^*(s)$, is developed in section 3.2 using the diffusive flux equation developed recently (Zhou, Oldenburg, Rutqvist, & Birkholzer, 2017; Zhou, Oldenburg, Spangler, & Birkholzer, 2017). With $G_0^*(x, s)$ and $g^*(s)$ available, the new dual-continuum solutions for heat transport in fractured reservoirs are developed using $G^*(x, s) \Rightarrow G_0^*\left(x, s\left[1 + \vartheta g^*(s)\right]\right)$ that is given in section 3.1.

This procedure of solution development is simple and different from that for traditional analytical solutions with step-by-step derivations (e.g., Bodvarsson & Tsang, 1982). In the latter, $sg^*(s)$ is obtained by solving the matrix temperature solution in the Laplace domain and taking its derivative with respect to the single space coordinate at the fracture-matrix interface for a specific 1-D matrix block (sphere, cylinder, or slab). Our solution procedure allows for an easy treatment of multirate heat transfer between fractures and matrix blocks of different shapes, sizes, properties, and volume fractions. In our procedure, the developments of $G_0^*(x, s)$ and $g^*(s)$ are completely separated and can be performed in parallel. The same solution procedure has been used for modeling solute transport in fractured and other dual-continuum media (Carrera et al., 1998; Dentz & Berkowitz, 2003; Haggerty et al., 2000).

3.1 Generalized Solutions $G^*(x, s)$ With Exchange Coupling

We use $G_0^*(x, s)$ to denote the analytical solutions to equation 4 with $\vartheta g^*(s) = 0$ and a Dirac delta heat pulse at the inlet boundary. Physically, $G_0^*(x, s)$ are the global transfer functions in the Laplace domain for convection, convection-conduction, and convection-dispersion in a single continuum (i.e., the fracture network) without coupling with matrix blocks.

The generalized solutions, $G^*(x, s)$, to the general heat equation in the Laplace domain, equation 4, with $\vartheta g^*(s) \neq 0$ can be written directly as follows:

$$G^*(x, s) = B^*(s) G_0^*\left\{x, s\left[1 + \vartheta g^*(s)\right]\right\}, \quad (9)$$

where x represents the longitudinal coordinate for 1-D linear, 1-D radial, and 2-D dipole systems and $B^*(s)$ is the subsidiary function for the inlet boundary

condition. For a fractured reservoir bounded by aquitards, the generalized solutions $G^*(x,s)$ can be written as follows:

$$G^*(x,s) = B^*(s)G_0^*\left(x, s\left[1 + \vartheta g^*(s) + \vartheta_{aa} g_{aa}^*(s)\right]\right), \quad (10)$$

where $\vartheta_{aa} = (\theta_f R_f)^{-1}$ and $g_{aa}^*(s)$ follows equation 5c.

For a Dirac delta heat pulse, $B^*(s) = 1$. For a constant unit temperature change, $B^*(s) = 1/s$. For a finite-duration unit temperature change, $B^*(s) = [1 - \exp(-t_D s)]/s$, where t_D is the time duration of the unit temperature change. The Laplace transform variable s in equations 9 and 10 is with respect to real time t.

Note that $g(t)$ and $g^*(s)$ are used to represent the linear system of the rock matrix for heat conduction, and $G_0(x,t)$ and $G_0^*(x,s)$ are used to represent the linear system of the fracture continuum only for heat convection, conduction, and dispersion in a given flow field. The system comprising the fractured reservoir including fracture continuum and matrix continuum represented by $G(x,t)$ and $G^*(x,s)$ is also linear for a given flow field. All of these functions are for the condition of a unit step temperature change at the inlet boundary. For any value of boundary temperature change, the corresponding solutions can be easily calculated using the superposition of linear systems, that is, $\Delta T G(x,t)$, where ΔT is the temperature change specified at the inlet boundary. This method is the same as the normalization of temperature in the step-by-step derivation of conventional solutions for boundary value problems.

3.2 Multirate Memory Function $g^*(s)$ for Fracture-Matrix Heat Exchange

To be consistent with the dual-continuum-based governing equations in section 2, we use the memory function $g(t)$ to represent the transient conductive heat flux through fracture-matrix interfaces per unit volume of REV of matrix blocks per unit temperature change in fractures. $g(t)$ can have contributions either from uniform matrix blocks of the same shape, size, and properties or from a collection of matrix blocks of different shape, size, properties, and volume fraction.

For a single matrix block of regular shape (sphere, cylinder, slab, square, rectangle, cube, and rectangular parallelepiped), we use the unified-form diffusive flux equation with the first-order approximation (Zhou, Oldenburg, Rutqvist, & Birkholzer, 2017; Zhou, Oldenburg, Spangler, & Birkholzer, 2017):

$$f_d(t_d) = \begin{cases} a_1/\sqrt{t_d} + a_2 + a_3\sqrt{t_d}, & t_d < t_{d0} \\ \sum_{j=1}^{N} b_{1j} b_{2j} \exp\left(-b_{2j} t_d\right), & t_d \geq t_{d0} \end{cases} \quad (11)$$

where f_d is the dimensionless transient flux with $\int_0^\infty f_d(t_d)dt_d = 1$, $t_d = D_m t/l^2$ is the dimensionless time, a_1, a_2, and a_3 are the parameters for the early-time polynomial solution $f_e(t_d)$, b_{1j}, b_{2j}, and N are the parameters for the late-time

exponential solution $f_l(t_d)$, and t_{d0} is the switchover dimensionless time for partitioning the entire time domain. $t_{d0} = 0.22$ is used for any shapes of matrix blocks. These parameters for various regular matrix blocks are given in Appendix B.

Equation 11 for matrix block k can be rewritten as follows:

$$f_d^k(t_d^k) = f_e^k(t_d^k) + U(t_d^k - t_{d0})\left[f_l^k(t_d^k) - f_e^k(t_d^k)\right], \quad (12)$$

where $U()$ is the Heaviside function that vanishes for negative values and is unity for positive values and f_e and f_l are the early-time and late-time solutions shown in equation 11.

Taking Laplace transforms of equation 12 with respect to dimensionless time t_d^k leads to the following:

$$f_d^{k*}(p) = \mathscr{L}_1 + \mathscr{L}_2 - \mathscr{L}_3, \quad (13a)$$

with the three terms on the right-hand side represented by

$$\mathscr{L}_1 = \mathscr{L}\left\{f_e^k(t_d^k)\right\} = \sqrt{\pi}a_1 p^{-1/2} + a_2 p^{-1} + \left(\sqrt{\pi}/2\right)a_3 p^{-3/2}, \quad (13b)$$

$$\mathscr{L}_2 = \mathscr{L}\left\{U(t_d^k - t_{d0})f_l^k(t_d^k)\right\} = \sum_{j=1}^{N} b_{1j}b_{2j}\exp\left[-(p+b_{2j})t_{d0}\right]/(p+b_{2j}), \quad (13c)$$

$$\mathscr{L}_3 = \mathscr{L}\left\{U(t_d^k - t_{d0})f_e^k(t_d^k)\right\} = a_1\mathscr{L}_4 + a_2 p^{-1}\exp(-pt_{d0}) + a_3\mathscr{L}_5, \quad (13d)$$

$$\mathscr{L}_4 = \sqrt{\pi}\left\{\frac{1-\tanh\sqrt{p}}{\sqrt{p}} + \frac{2\exp[-(p+\pi^2/4)t_{d0}]}{p+\pi^2/4}\right\}, \quad (13e)$$

$$\mathscr{L}_5 = \frac{1}{a_3^c}\left\{\left[\mathscr{L}_1^c + \frac{4\exp\left[-(p+\beta_1^2)t_{d0}\right]}{p+\beta_1^2} - \frac{2}{\sqrt{p}}\frac{I_0(\sqrt{p})}{I_1(\sqrt{p})}\right] - a_1^c\mathscr{L}_4 - a_2^c p^{-1}\exp(-pt_{d0})\right\}. \quad (13f)$$

where p is the Laplace variable with respect to t_d^k, superscript c denotes the parameter values for a cylinder (see Appendix B), I_0 and I_1 are the modified Bessel functions of the first kind of the zeroth and first order, respectively, and β_1 (=2.4048255577) is the first positive root of the Bessel function of the first kind of order zero. The derivation of $\mathscr{L}_3$ is detailed in Appendix C.

We finally take Laplace transforms of equation 5a and obtain

$$g^*(s) = \sum_{k=1}^{K}\left[w_m^k R_m^k \frac{D_m^k}{(l^k)^2}\right]\mathscr{L}\left\{f_d^k(t_d^k)\right\} = \sum_{k=1}^{K} w_m^k R_m^k f_d^{k*}(p), \quad (14)$$

where $p = s/\left[D_m^k/(l^k)^2\right]$. Equation 14, along with equations 13a–13f, is used to calculate the memory function $g^*(s)$ for multirate fracture-matrix heat transfer. Note that $g^*(s)$ is dimensionless, unlike $g(t)$ that has dimensions of inverse time.

3.3 Global Transfer Functions $G_0^*(x,s)$ Without Coupling

In this section, we list a number of independent $G_0^*(x,s)$, that is, the solutions for heat transport in a single continuum under 1-D linear, 1-D radially

diverging, and 2-D dipole flow. The fundamental boundary conditions include (1) a Dirac delta heat pulse at the inlet boundary (i.e., $x = 0$ for 1-D linear flow or at $r = r_w$ for a 1-D diverging and 2-D dipole flow, where r_w is the radius of the injection well) and (2) no temperature perturbation at $x = +\infty$ or $r = +\infty$.

3.3.1 One-Dimensional Linear Flow

The subsidiary equation for heat transport in 1-D linear flow, equation A2, with $g^*(s) = 0$ is a second-order ordinary differential equation, and its solution can be directly written (Avdonin, 1964a; Sudicky & Frind, 1982; Tang et al., 1981):

$$G_0^*(x,s) = \exp\left\{\frac{\phi_f}{R_f}\frac{P_e}{2}\left\{1-\left[1+\left(\frac{R_f}{\phi_f}\right)^2\frac{4}{P_e}\tau s\right]^{1/2}\right\}\right\}, \quad (15a)$$

with

$$\tau = x/u_f, \quad P_e = u_f x/D_{ef} \quad (15b)$$

where τ is the mean residence time and P_e is the Peclet number with respect to the flow length scale x. The velocity u_f in the 1-D linear flow is constant and the dispersion-induced thermal diffusivity D_{df} is thus constant, leading to a constant effective thermal diffusivity D_{ef}. Equations 15a and 15b are applicable for any combinations of intrinsic thermal diffusivity D_f and dispersion-induced thermal diffusivity D_{df}.

In the case of dominant convection with negligible D_{ef} (Lauwerier, 1955), equation A2 degrades to a first-order ordinary differential equation, and the solution is simplified to

$$G_0^*(x,s) = \exp\left\{-\frac{R_f}{\phi_f}\tau s\right\}, \quad (16)$$

with $\tau = x/u_f$.

3.3.2 One-Dimensional Radially Diverging Flow

In the case of no thermal dispersion with $D_{ef} = D_f$, the solution to the subsidiary equation for heat transport, equation A5, with $g^*(s) = 0$ can be written (Avdonin, 1964a; Carslaw & Jaeger, 1959, p. 389; Chen & Reddell, 1983) as follows:

$$G_0^*(r,s) = \frac{2^{1-\nu}}{\Gamma(\nu)}\left(r\sqrt{\frac{s}{D_{ef}}}\right)^{\nu} K_\nu\left\{r\sqrt{\frac{s}{D_{ef}}}\right\}, \quad (17)$$

where K_ν is the modified Bessel function of the second kind with order ν and Γ is the gamma function. The solution in equation 17 can be rewritten as follows:

$$G_0^*(r,s)=\frac{2^{1-\nu}}{\Gamma(\nu)}\left[\sqrt{\frac{2P_e}{(1-r_{wd}^2)}}\sqrt{\tau s}\right]^{\nu}K_{\nu}\left\{\sqrt{\frac{2P_e}{(1-r_{wd}^2)}}\sqrt{\tau s}\right\},\quad(18a)$$

in terms of the mean residence time τ calculated by

$$\tau=\int_{r_w}^{r}\frac{dr}{u_f(r)}=\frac{\phi_f}{2Q'}\left(r^2-r_w^2\right),\quad(18b)$$

the constant Peclet number P_e calculated by

$$P_e=u_f r/D_{ef}=Q'/\phi_f D_f,\quad(18c)$$

and the dimensionless number ν defined by

$$\nu=\frac{\phi_f}{2R_f}P_e,\quad(18d)$$

where the dimensionless well radius $r_{wd}=r_w/r$.

In the case of dominant dispersion-induced thermal diffusivity with $D_{ef}\approx D_{df}=\alpha_L u_f/R_f$, the solution to the subsidiary equation for heat transport, equation A8, with $g^*(s)=0$ can be written (Chen, 1985; Moench & Ogata, 1981; Reimus et al., 2003; Tang & Babu, 1979):

$$\begin{cases} G_0^*(\varrho,s)=\exp\left(\frac{y-y_w}{2}\right)\dfrac{\mathrm{Ai}\left(\frac{1}{\beta^3}y\right)}{\mathrm{Ai}\left(\frac{1}{\beta^3}y_w\right)} \\ y=\varrho+(4\beta)^{-1},y_w=\varrho_w+(4\beta)^{-1} \\ \varrho=\phi_f r/\alpha_L,\varrho_w=\phi_f r_w/\alpha_L \\ \beta=\dfrac{R_f\alpha_L^2}{Q'\phi_f^2}s \end{cases}\quad(19)$$

where $Ai()$ is the Airy function of the first kind (Abramowitz & Stegun, 1972). We introduce the Peclet number $P_e=u_f r/(\alpha_f u_f/R_f)=R_f r/\alpha_L$ and the mean residence time in equation 18b. The solution in equation 19 can be rewritten as follows:

$$\begin{cases} G_0^*(\varrho, s) = \exp\left[\dfrac{\phi_f P_e}{R_f\, 2}(1-r_{wd})\right] \dfrac{\mathrm{Ai}\left(\overline{\beta^3 y}^{\,-1}\right)}{\mathrm{Ai}\left(\overline{\beta^3 y_w}^{\,-1}\right)} \\ y = \varrho + (4\beta)^{-1}, y_w = \varrho_w + (4\beta)^{-1} \\ \varrho = \dfrac{\phi_f}{R_f} P_e, \varrho_w = \dfrac{\phi_f}{R_f} P_e r_{wd} \\ \beta = \left(\dfrac{R_f}{\phi_f}\right)^3 \dfrac{2}{P_e^2(1-r_{wd}^2)} \tau s \end{cases} \quad (20)$$

In the case of dominant convection with negligible D_{ef} (Bodvarsson & Tsang, 1982; Malofeev, 1960), equation 16 works with the mean residence time calculated by equation 18b.

3.3.3 Two-Dimensional Dipole Flow

It is assumed that $G_0^*(x, s)$ in equation 15a for 1-D linear flow is applicable for the convective-conductive-dispersive heat transport along each streamline between the injection well and the withdrawal well. The mean residence time and the length, L, for the streamline with a given central angle ω (Alishaev, 1979; Gringarten & Sauty, 1975; Grove & Beetem, 1971), as well as the Peclet number, can be calculated as follows:

$$\tau = \frac{4\pi\phi_f d^2 B_f}{Q\sin^2\omega}(\omega\cot\omega - 1), \quad L = \frac{2d\omega}{\sin\omega}, \quad P_e = \frac{L}{\alpha_L}, \quad (21)$$

where d is the half-distance between the two wells. The central angle ω is formed between the central line of the two wells and the straight line connecting a point on the central line and the injection well. In this case, the dispersion-induced thermal diffusivity is dominant with $D_{ef} \approx \alpha_L u_f / R_f$ and the Peclet number, one of the two key parameters, is constant, even though the velocity and thermal diffusivity vary along the streamline.

In the case of negligible thermal dispersion, $D_{ef}(=D_f)$ is constant, and thus, P_e is variable along the streamline. An effective Peclet number with a mean velocity may be used to minimize the approximation errors, while still using the same solution for 1-D linear flow.

Similarly, the solution in equation 15a with equation 21 is applicable for a stream tube with the central angle in the range $[\omega - 0.5\Delta\omega, \omega + 0.5\Delta\omega]$. The entire 2-D flow field can be represented by n_s stream tubes, each with the identical angle increment between the two bounding streamlines: $\Delta\omega = \pi/n_s$. The thermal breakthrough curve at the withdrawal well can be obtained by flux weighting the breakthrough curve for each stream tube. This solution for

either dominant or negligible dispersion-induced thermal diffusivity may result in two types of approximation errors. The first type of approximation error is caused by the nonconstant Peclet number along each streamline and can be evaluated using numerical particle tracking (Zhou et al., 2007) along the streamline with each tracked streamline segment represented by constant velocity and equations A1 and A2. The second type of approximation error is caused by the assumption of no heat exchange between different stream tubes and can be evaluated using high-resolution numerical simulations.

For the single-well injection-withdrawal (SWIW) flow, the solutions to equations A9 and A10 are complicated in the case of $g^*(s) = 0$ because equations A9 and A10 are inhomogeneous ordinary differential equations. The generalized solutions with $g^*(s) \neq 0$ are more complicated because of the contributions from the nonuniform initial matrix temperature for the withdrawal period. These solutions are beyond the scope of the paper and will be included in future work.

3.3.4 A Note on the Similarity Between Heat and Solute Transport

The global transfer functions $G_0^*(x,s)$ presented above have the same functional forms as those for solute transport in fractures or fractured reservoirs, with the same physical definitions of the mean residence time and the Peclet number. There are the following correspondences between the mean residence time, τ^S, and the Peclet number, P_e^S, for solute transport and those for heat transport:

$$R_f^S \tau^S = \frac{R_f}{\phi_f}\tau, \text{and } P_e^S = \frac{\phi_f}{R_f} P_e. \quad (22)$$

With these correspondences, equation 15a is identical to equation 23 in Tang et al. (1981), equation 19 in Sudicky and Frind (1982), equation (A6) in Reimus et al. (2003), and equation (1) in Hawkins et al. (2017) for 1-D linear flow and solute transport, while equation 20 is identical to equation (A7) in Reimus et al. (2003) and equations A9 and A10 in Zhou et al. (2007) for 1-D radial advective-dispersive solute transport.

As shown in equations 16 and 22, the (actual) retardation factor for heat transport in fractures is $R_f^{'} = \frac{R_f}{\phi_f}$. For example, $R_f^{'} = 1.07$ for the fractures with parameters listed in Table 1, while $R_m^{'} = \frac{R_m}{\phi_m} = 3.525$ if the rock matrix is the single continuum for heat transport. The thermal retardation factor denotes the ratio of the fracture (or matrix) heat capacity to flowing-water heat capacity in the pore space per unit volume of fracture (or matrix) media: $R_f^{'} = \rho_f c_f / \phi_f \rho_w c_w$ ($R_m^{'} = \rho_m c_m / \phi_m \rho_w c_w$). The difference between solute and thermal retardation factors can be attributed to the nature of heat storage which occurs in both pores and grains while solute storage occurs only in pores. Similarly, the difference between P_e and P_e^S is caused by (1) that P_e is the ratio of convective heat transport in the pore space to the conductive

heat transport in the continuum with the pore space and grains and (2) that P_e^S is the ratio of advective to dispersive solute transport, all within the pore space in a continuum.

Table 1
Grain and Water Thermal Properties, Rock Properties of the Fracture and Matrix Continua, and Model Parameters for the Fluid Flow, Reservoir, and Aquitards, As Well As Their Ranges for Sensitivity Analysis

Rock parameters	Value
Density of solid grains ρ_g	2,650 kg/m^3
Specific heat of solid grains c_g	1,000 J·kg^{-1}·°C^{-1}
Thermal conductivity of wet grains λ_m	2.50 W·m^{-1}·°C^{-1}
Density of water ρ_w	1,000 kg/m^3
Specific heat of water c_w	4,200 J·kg^{-1}·°C^{-1}
Thermal conductivity of water λ_w	0.615 W·m^{-1}·°C^{-1}
Volume fraction of fractures θ_f	0.01
Intrinsic porosity of fractures ϕ_f	0.90
Enhancement factor of fractures R_f	0.963
Thermal diffusivity of fractures D_f	1.52×10^{-7} m^2/s
Retardation factor of fractures R_f/ϕ_f	1.07
Volume fraction of the matrix θ_m	0.99
Intrinsic porosity of the matrix ϕ_m	0.20
Enhancement factor of the matrix R_m	0.705
Thermal diffusivity of the matrix D_m	8.45×10^{-7} m^2/s
Retardation factor of the matrix R_m/ϕ_m	3.525
Fracture-matrix scaling factor ϑ	102.80
Fracture-matrix retardation factor $(1 + \vartheta R_m)R_f/\phi_f$	78.62
Fracture velocity for linear flow u_f	10^{-2}, 10^{-3}, 10^{-4} m/s
Injection rate for radial flow Q	0.0634 m^3 s^{-1} (2×10^6 m^3/year)
Longitudinal thermal dispersivity of fractures α_L	0, 0.01, 0.1, 1 m
Reservoir thickness B_f	20 m
Aquitard thickness B_a	30, 50 m
Water-convection distance L	100 m

Due to the intrinsic thermal diffusivity of matrix blocks being orders of magnitude higher than the solute coefficient of matrix diffusion, fractures and matrix blocks with a small fracture half-spacing may reach thermal equilibrium after a sufficient time. In this case, the retardation factor is

$$R_{fm}^{'} = \frac{R_f}{\phi_f}(1 + \vartheta R_m), \quad (23)$$

which can be used to estimate the travel distance of the thermal front relative to the fracture water front.

The similarity of global transfer functions between heat and solute transport in fractured reservoirs has not been widely recognized by the two (heat- and solute-transport) modeling communities. For example, the solute-transport solution of Tang et al. (1981) without solute decay is the same as the heat-transport solution of Avdonin (1964a). The former considers a single fracture with an embedded infinite matrix, while the latter deals with a single aquifer bounded by two semi-infinite aquitards. On the other hand, the recent advances in modeling solute transport have not been introduced to the heat-transport modeling community, including (1) the analog between thermal and solute dispersion and (2) the concept of transfer and memory functions. Indeed, the generalized memory function presented in section 3.2 is applicable to the exchange by heat conduction, solute diffusion, and hydraulic diffusion between fractures and the matrix and between aquifers and aquitards.

3.4 SHPALib

We coded the above solutions with the global transfer functions and the generalized memory function into a Fortran package, referred to as SHPALib (Solute and Heat Transport and Pressure Propagation: An Analytical Solutions Library). The SHPALib extends to heat-transport modeling from the TRAT code that was developed for analytical modeling of tracer transport in fractured reservoirs (Zhou et al., 2007). The TRAT code was developed based on the Fortran code in Moench (1995) and was extended for pressure propagation (Zhou et al., 2009). The SHPALib also includes the subroutines for unified-form diffusive flux equations for various matrix blocks and intrablock solutions of solute, heat, and pressure transport (Zhou, Oldenburg, Rutqvist, & Birkholzer, 2017; Zhou, Oldenburg, Spangler, & Birkholzer, 2017).

Because of the complexity of the memory function $g^*(s)$, there are no analytical Laplace inversions available for the solutions, $G^*(x, s)$. We use the method developed by de Hoog et al. (1982) for efficient numerical inversion of Laplace transforms. This method has been widely used for analytical modeling of pressure propagation (e.g., Zhou et al., 2009), tracer transport (e.g., Moench, 1995; Zhou et al., 2007), and heat transport (Ruiz Martínez et al., 2014; Yang & Yeh, 2009).

In this study, SHPALib was tested by numerically inverting memory function $g^*(s)$ in equations 13a–13f and 14 for a slab, three rectangles, and three rectangular parallelepipeds with different (R_{I2}, R_{I3}) (see equation B6), all matrix blocks with identical minimum half-spacing and thermal diffusivity. The true solutions of the diffusive flux for these matrix blocks were calculated using the diffusive flux equations 11 and B1–B7 in the real-time domain. Note that a unit temperature change was specified at the surrounding fractures and a uniform initial temperature was specified for the matrix blocks. As shown in Figure 2, excellent agreement is obtained in all of the cases between the analytical solutions in the real-time domain and the semianalytical solutions with Laplace transform and inversion, indicating that

the memory function $g^*(s)$ in equations 13a–13f and 14 and the inversion algorithm of Laplace transforms work properly.

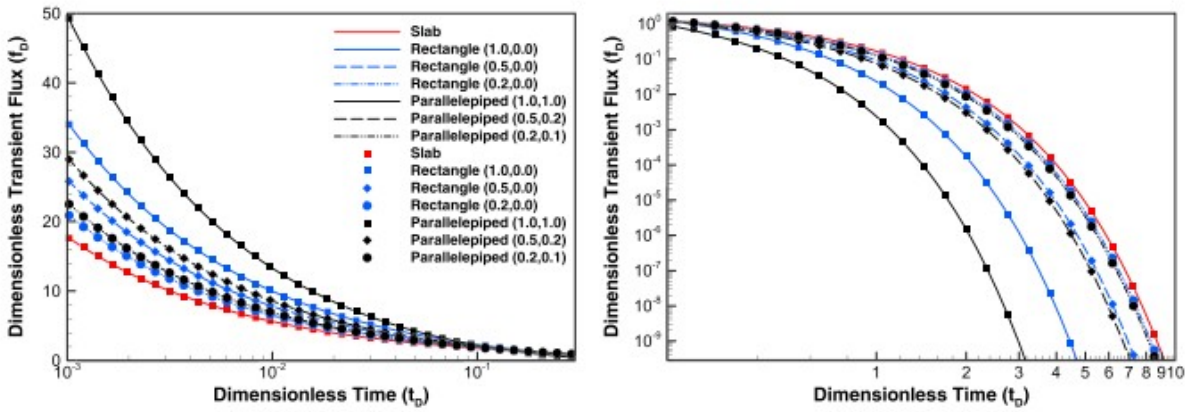

Figure 2. Comparison between the dimensionless transient flux calculated by the diffusive flux equations in the real-time domain (lines) and by numerically inverting the generalized memory function (symbols) for seven 1-D, 2-D, and 3-D matrix blocks.

4 Benchmark Examples

The developed analytical solutions were demonstrated for three heat-transport benchmark problems: a single-continuum reservoir, a fractured reservoir, and a fractured reservoir bounded by aquitards, with or without the A-A (aquifer-aquitard) and F-M (fracture-matrix) coupling. By comparison, these problems were used to better understand the retardation of heat transport in fractures by the rock matrix and aquitards. For each benchmark problem, a number of sensitivity analyses were conducted for fluid-flow fields (1-D linear and radial), heat-transport mechanisms (convection, conduction, and dispersion), shape and size of matrix blocks, and key model parameters. Here, we considered reservoirs with a thickness of B_f = 20 m. For radial flow, a realistic injection rate of $Q = 2 \times 10^6$ m^3/year for geothermal fields and the operations of aquifer thermal energy storage was used, with fracture pore velocity of u_f = 0.01, 0.001, and 0.0001 m/s at a distance of 5, 50, and 500 m, respectively. For linear flow, the three velocities were used for sensitivity analysis. For transport mechanisms, four longitudinal dispersivities α_L = 0, 0.01, 0.1, and 1 m were considered, along with the case of convection only with D_{ef} = 0. A unit temperature change was specified at the inlet or well boundary and a uniform initial temperature was specified for the systems.

For the sensitivity analyses of fracture-matrix heat exchange, seven matrix blocks of uniform sizes and three values of minimum fracture half-spacing l = 0.2, 1, and 5 m were used for single-rate heat exchange. The matrix blocks include (1) a slab, (2) three rectangles with (R_{l2}, R_{l3}) pairs with values (1.0, 0.0), (0.5, 0.0), and (0.2, 0.0), and (3) three rectangular parallelepipeds with (R_{l2}, R_{l3}) equal to (1.0, 1.0), (0.5, 0.2), and (0.2, 0.1). For multirate heat exchange, five collections of matrix blocks of different shapes

and sizes were used. The first two collections consist of either three 2-D or three 3-D rectangular matrix blocks above with the same l values, and the last three collections consist of (1) three 2-D, (2) three 3-D, and (3) six 2-D and 3-D rectangular matrix blocks above with l = 0.2, 1, and 5 m mixed. The volumetric fraction of each component matrix block in the five collections is 1/3, 1/3, 1/9, 1/9, and 1/18, respectively.

A water-convection distance of 100 m was used for comparison among the different cases of sensitivity analyses. The transport time for observation was accordingly determined for each velocity and flow field, and the different times were used to investigate the different regimes of fracture-matrix heat exchange. Table 1 lists relevant rock and model parameters.

4.1 Heat Transport in Single-Continuum Reservoirs Without Coupling

In this example, we are interested in heat-transport mechanisms in a single-continuum reservoir without the A-A and F-M coupling. For linear flow in the single-continuum reservoir (i.e., the matrix continuum with $\theta_m = 1$), three pore velocities: $u = 0.5 \times 10^{-3}$, 0.5×10^{-4}, and 0.5×10^{-5} m/s (matrix porosity is 0.2) are used and the corresponding transport time for observation is 2.315, 23.15, and 231.5 days. The effective thermal diffusivity is calculated using $D_{em} = D_m + \alpha_L u = 8.45 \times 10^{-7} + \alpha_L u$ m^2/s. In addition, twelve cases for fractures (i.e., the fracture continuum with $\theta_f = 1$) are considered with three pore velocities: $u = 10^{-2}$, 10^{-3}, and 10^{-4} m/s and the above four dispersivities. The effective thermal diffusivity is calculated using $D_{ef} = D_f + \alpha_L u = 1.52 \times 10^{-7} + \alpha_L u$ m^2/s. The corresponding transport time is 0.116, 1.16, and 11.6 days, respectively.

Figure 3 shows the temperature profiles centered (with a relative distance of 0) at the same distance scaled by the actual thermal retardation factor $R_m^{'} = R_m/\phi_m$ (or $R_f^{'} = R_f/\phi_f$) for the 12 cases in the matrix (or fracture) continuum. The relative distance of 0 is located at the heat-convection distance with thermal retardation, which is 28.37 m for the matrix continuum and 93.46 m for the fracture continuum. These heat-convection distances show the effects of thermal retardation by the conductive solid grains in the matrix and the fractures when comparing to the water-convection distance of 100.0 m. The retardation factor for the matrix is $R_m^{'} = 3.525$, leading to significant thermal retardation caused by local equilibrium between water and solid grains. The retardation factor for fractures is $R_f^{'} = 1.07$, leading to moderate thermal retardation.

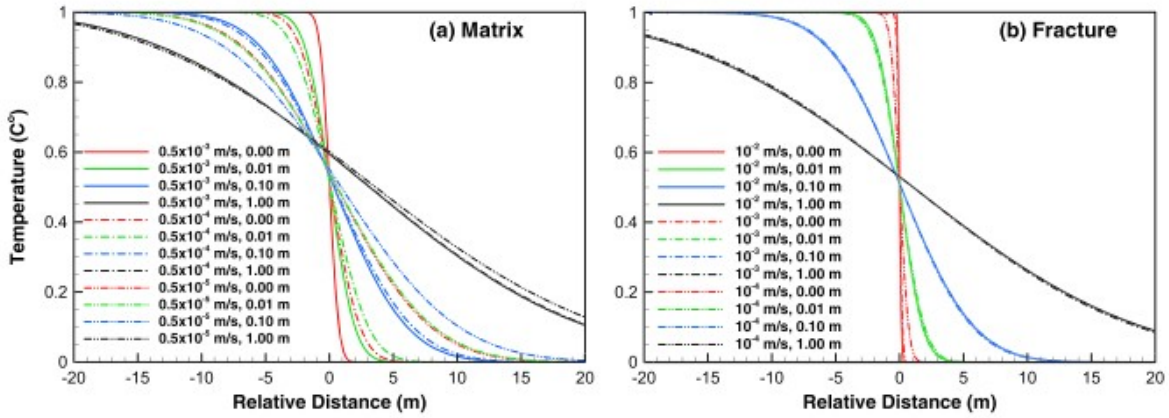

Figure 3. Temperature profiles centered (with a relative distance of 0) at (a) 28.37 m for the matrix continuum and (b) 93.46 m for the fracture continuum, as a function of thermal dispersivity, with the three pore velocities of linear flow. The data pair in the legends are pore velocity and longitudinal dispersivity α_L.

As shown in Figure 3a, thermal dispersion has a significant effect on temperature profiles for the matrix in each velocity case, showing a larger spreading (defined here by the distance between $T = 0.98$ and 0.02) for a higher longitudinal dispersivity. The spreading is 2.4, 7.4, and 22.2 m in the three velocity cases with no dispersion, while it varies slightly from 52.4 to 55.8 m in the cases of $\alpha_L = 1$ m. In the latter, P_e for the heat-convection distance varies slightly from 28.3 to 24.3, leading to similar temperature profiles for the three velocities. In all cases of lower α_L, a stronger effect of pore velocity on P_e and thus on temperature profiles is observed because of less dominance of heat dispersion over heat conduction. Note that the temperature at the relative distance of 0 is not 0.5 in some cases because of the effect of the fixed-temperature condition at the inlet (Kreft & Zuber, 1978; Ogata & Banks, 1961).

As shown in Figure 3b, thermal dispersion also has a significant effect on temperature profiles for fractures in all velocity cases. In the cases of $\alpha_L = 1$ m, thermal dispersion is dominant in the effective thermal diffusivity because of higher velocities than those for the matrix, leading to identical P_e (=93.46) and identical temperature profiles with a spreading over 55 m in the three velocity cases. In the cases with convection-conduction only, P_e is very large (6.16×10^6, 6.16×10^5, and 6.16×10^4), leading to slightly different but sharp profiles with a spreading of less than 2.0 m. These sharp profiles are similar to the step function (with transition from 1 to 0) without thermal conduction and dispersion. In the other two cases of α_L, the spreading is 6.0 and 18.0 m. The temperature profiles calculated above for fractures only are the envelopes of those calculated for heat transport in a fractured reservoir with the F-M coupling (to be discussed below).

4.2 Heat Transport in Fractured Reservoirs

In this example, we focus on (1) effective thermal diffusivity and (2) single-rate and multirate heat exchange between fractures and matrix blocks and related effects on global convective-conductive-dispersive heat transport in a fractured reservoir under 1-D linear and radial flow.

4.2.1 One-Dimensional Linear Fluid Flow

Convective-conductive or convective-conductive-dispersive heat transport is simulated using equations 15a and 15b, and the convective heat transport is simulated using equation 16, along with the memory function in equations 13a–13f and 14 and the generalized solution in equation 9. Figure 4 shows the profiles of fracture temperature, as functions of effective thermal diffusivity, shape of isotropic matrix blocks (slabs, squares, and cubes), and l (0.2, 1, and 5 m) of the matrix blocks, in the three cases of fracture velocity. Note that the solutions for α_L = 0.01 m and convection only (not shown) are almost identical to those with intrinsic thermal diffusivity (D_f).

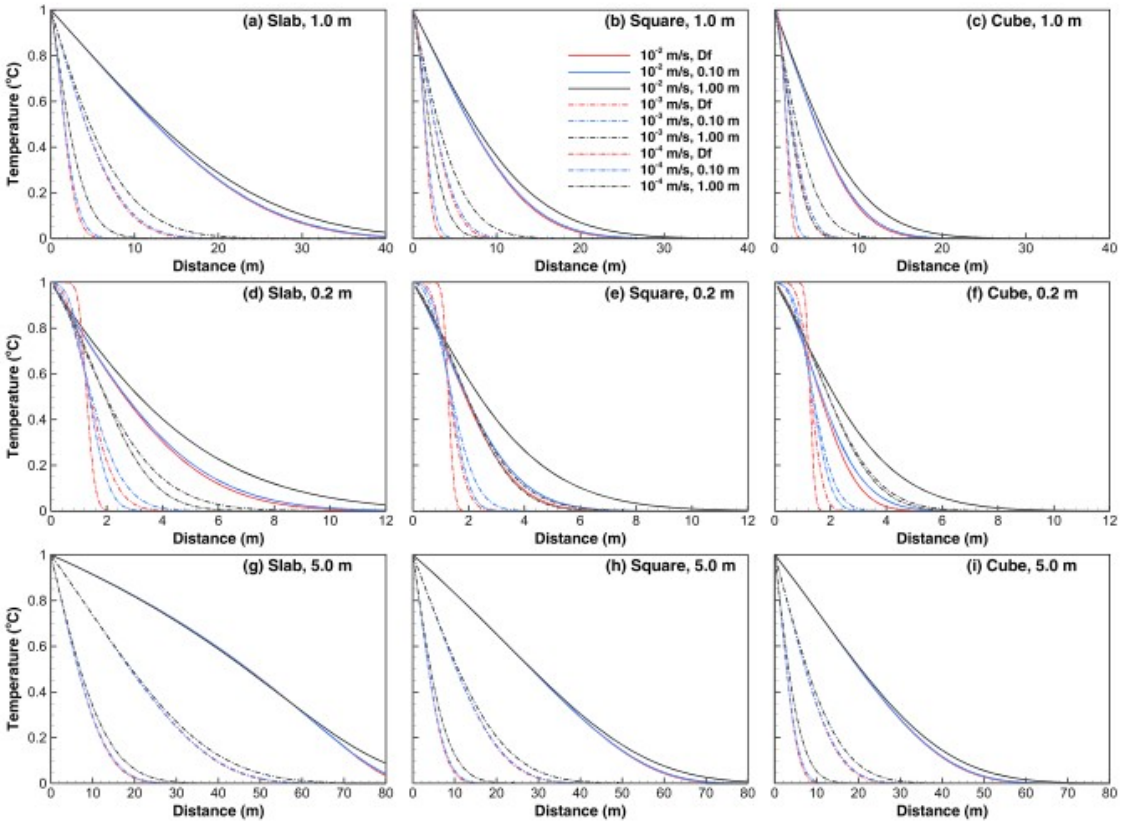

Figure 4. (a–i) Fracture temperature profiles, as functions of longitudinal dispersivity (0.0, 0.1, 1.0 m), and shape (slabs, squares, and cubes) and l (0.2, 1, and 5 m) of uniform matrix blocks, for the three fracture velocities of linear fluid flow.

Thermal dispersion in fractures has a moderate impact on temperature profiles as shown by the difference between α_L = 1 m and α_L = 0.1 m in all cases of matrix blocks. It appears that the relative difference increases with the reduction in l from 5.0 to 0.2 m. For an effective thermal diffusivity

smaller than that with $\alpha_L \leq 0.1$ m, the temperature profiles are almost identical, indicating that the convection-conduction and convection-conduction-dispersion solutions for the fracture continuum can be approximated by the convection solutions (e.g., Bodvarsson & Tsang, 1982; Jung & Pruess, 2012; Lauwerier, 1955). This conclusion may not be valid for the single fracture or matrix continuum (see Figure 3), indicating that the fracture-matrix heat exchange overshadows the effect of heat conduction and dispersion in fractures.

The shape and size of matrix blocks have a more significant effect on the profiles of fracture temperature, reducing the penetration depth in fractures and changing the shape of temperature profiles. The effect increases with the enhancement of the fracture-matrix heat exchange by the dimensionality of matrix blocks from 1 (slabs) to 3 (cubes) and by the reduction in l. The effect also depends on the velocity-dependent transport time that allows heat exchange to take effect, which is different from the negligible effect for the fracture continuum only without the F-M coupling (see Figure 3b). The block shape and size and transport time together determine the regimes of fracture-matrix heat exchange: the early-time regime when dimensionless time $t_d \leq 0.22$ or the equilibrium regime when $t_d \geq 2.0$ (Zhou, Oldenburg, Spangler, & Birkholzer, 2017). During the equilibrium regime, matrix and fracture temperatures are at quasi-equilibrium, and the additional effect of matrix blocks is negligible. In this case, the fracture temperature profiles become sharp again, slowed by a retardation factor of $R'_{fm} = \frac{R_f}{\phi_f}(1 + \vartheta R_m) = 78.62$ relative to fracture water convection. For example, the temperature profiles are centered at 1.27 m in the cases with pore velocity of 10^{-4} m/s, transport time of 11.6 days, $l = 0.2$ m, and $t_d = 21.2$ (see Figures 4d–4f).

Figure 5 shows the profiles of fracture temperature for four (anisotropic) rectangular matrix blocks with different aspect ratios (R_{l2}, R_{l3}) and five collections of matrix blocks for the three fracture velocities (0.01, 0.001, 0.0001 m/s) with $\alpha_L = 1$ m. As shown in Figure 5a for $l = 5$ m, the aspect ratios of matrix blocks affect temperature profiles in the three cases of velocity because matrix conduction (thermal diffusion) is in the early-time regime (see equation 11) with $t_d \leq 0.034$. This effect disappears in Figures 5b and 5c for $l = 0.2$, 1 m in some velocity cases with $t_d \gg 0.22$. The same is true for the two collections of 2-D and 3-D rectangular matrix blocks. The variations of fracture temperature in the six cases are bounded by the temperature profiles of cubes and slabs (see Figure 4). As shown in Figure 5d, fracture temperatures for the three collections with mixed aspect ratios and l values are impacted most by the matrix blocks with smallest l value (0.2 m) and largest aspect ratios (1.0). The effect can be seen from the comparison between the resulting temperature profiles and those for the collections with uniform $l = 0.2$ m and $l = 5.0$ m for the velocity of 0.0001 m/s. This is because the matrix blocks with $l = 0.2$ m are at

thermal equilibrium with fractures at the time scale of 11.6 days, significantly retarding the penetration depth of fracture temperature.

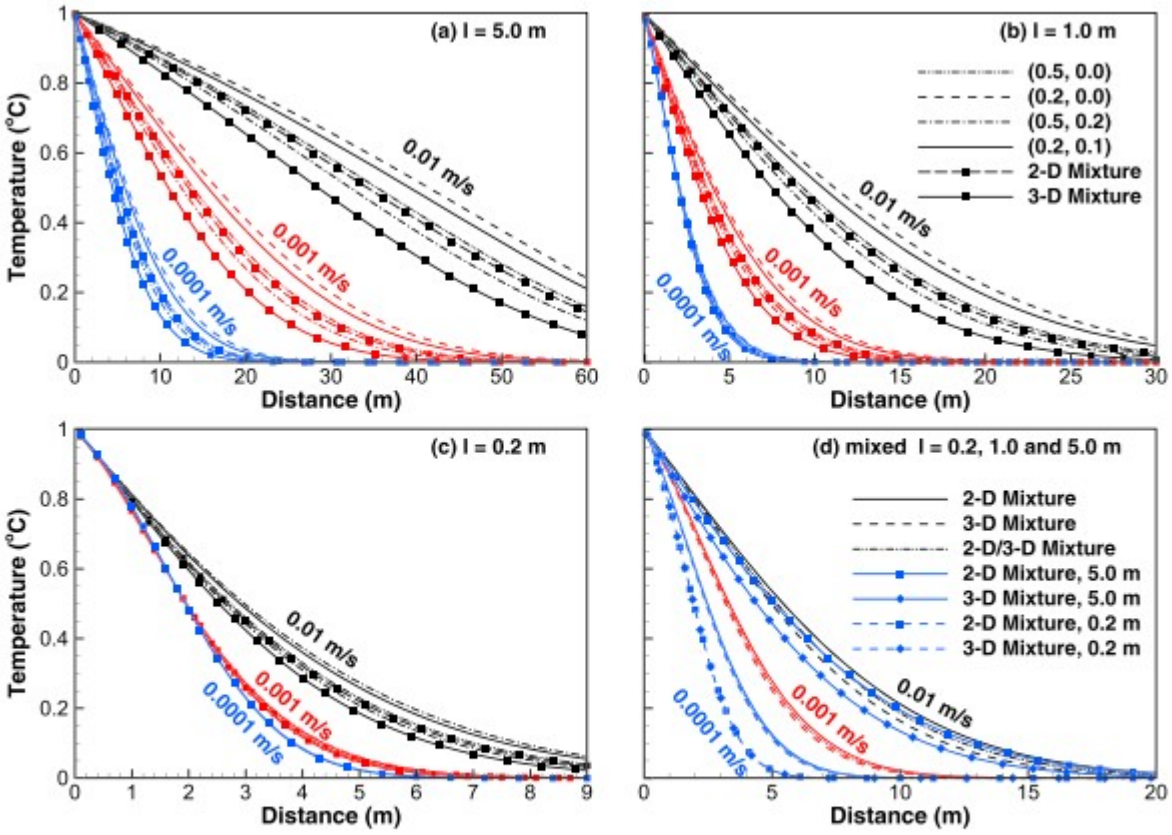

Figure 5. Fracture temperature profiles, as functions of (a–c) aspect ratios (R_{l2}, R_{l3}) of uniform rectangular matrix blocks and uniform collections of 2-D or 3-D rectangular blocks and l = 0.2, 1,and 5 m and (d) three collections of rectangular matrix blocks with mixed l, for fracture velocity of 0.01 m/s (black lines), 0.001 m/s (red lines), and 0.0001 m/s (blue lines) in linear fluid flow.

4.2.2 One-Dimensional Radial Fluid Flow

For 1-D radial flow, we also focus on the effects of effective thermal diffusivity and shape and size of matrix blocks on heat transport using (1) heat convection with solutions of equation 16 and (2) heat convection-dispersion with α_L = 0.01, 0.1, and 1 m with solutions of equation 20. The transport time for observation is 103.3 days calculated using equation 18b, and the lowest P_e at a radial distance of 100.0 m is 96.3. Only three isotropic matrix blocks (slabs, squares, and cubes) with l = 0.2, 1, and 5 m are considered as these cases produce bounding temperature profiles for anisotropic matrix blocks and collections of matrix blocks of identical l.

As shown in Figure 6, the profiles of fracture temperature in radial flow with a longer transport time are very different from those in the linear flow with shorter transport times in all of the cases of effective thermal diffusivity, shape, and l of matrix blocks. For the transport time of

103.3 days, t_d = 188.5, 7.54, and 0.30 for l = 0.2, 1.0, and 5.0 values, respectively. For l = 0.2 m and convection only, the temperature fronts for slabs, squares, and cubes are identically sharp with $T_f \approx 1$ ˚C at $r \leq 11.28$ m, with $R'_{fm} = 78.62$, indicating that fractures and matrix blocks are at equilibrium at $r \leq 11.28$ m. The temperature profile for l = 0.2 m is affected only by thermal dispersion, with the spreading of 12.1 m for α_L = 1.0 m.
For l = 1.0 m, the spreading is between [4.3 m, 18.1 m] for α_L = 1.0 m, without any effect of block shape, while it is [7.9 m, 14.8 m] for convection only, with a small effect of block shape. For l = 5.0 m, the spreading for convection only varies from [3.0 m, 27.2 m] for slabs to [3.3 m, 21.3 m] for squares to [3.9 m, 18.8 m] for cubes, indicating the shape of matrix blocks affects the thermal penetration depth in fractures. For these wider spreadings, thermal dispersion only slightly affects the smeared temperature profiles. Note that the thermal penetration depth in fractures is significantly impacted by block size, thermal dispersion, and block shape in radial flow, and the fracture-matrix heat exchange significantly retards thermal fronts, limiting the penetration depth to less than 30 m in all the cases.

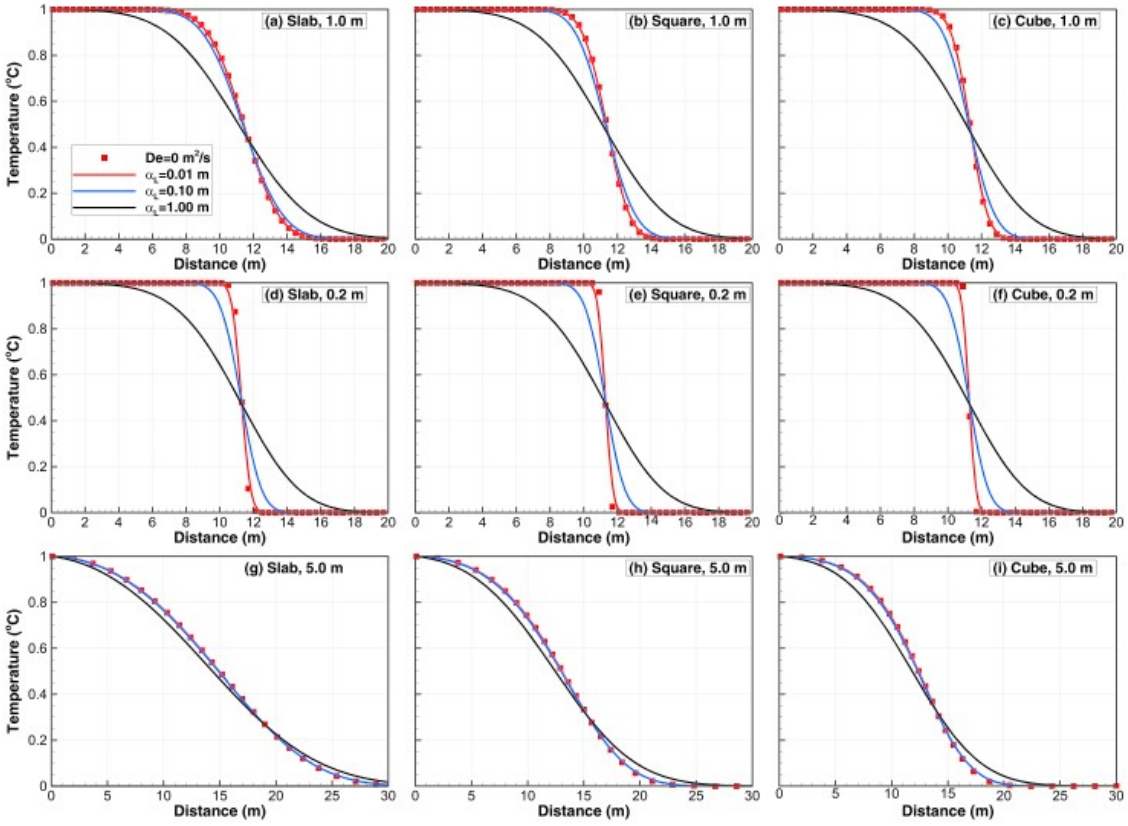

Figure 6. (a–i) Fracture temperature profiles, as functions of longitudinal dispersivity (0.01, 0.1, and 1.0 m) and convection only, and shape (slabs, squares, and cubes) and l (0.2, 1, and 5 m) of uniform matrix blocks, for the radial fluid flow with an injection rate of 2×10^6 m^3/year and a transport time of 103.3 days.

In the case of $\alpha_L \leq 0.01$ m, the global transfer function of convection only in fractures, equation 16, can be used with high accuracy for simplification of equation 18a or 20. The thermal penetration depth in all of the cases is less

than 30 m, where fracture velocity is $u_f = 1.68 \times 10^{-3}$ m/s and the dispersion-induced thermal diffusivity is $\alpha_L u_f / R_f = 1.74 \times 10^{-5}$ m^2/s for $\alpha_L = 0.01$ m, 2 orders of magnitude higher than intrinsic thermal diffusivity. This means that in the radial extent of thermal perturbations, intrinsic thermal diffusivity in fractures is negligible and its effect on fracture temperature can be neglected because of strong fracture-matrix heat exchange.

4.3 Heat Transport in Fractured Reservoirs Bounded by Aquitards

This example is used to demonstrate the flexibility of the developed analytical solutions in equation 10 when simultaneously handling both fracture-matrix and aquifer-aquitard systems. We add the upper aquitard with $B_a^1 = 30$ m and the lower aquitard with $B_a^2 = 50$ m to the fractured reservoir with a thickness of 20 m, with no heat flow condition on the other sides of the half-aquitards. The aquitards are assumed to have the same properties as the rock matrix of the reservoir. As shown in Figure 7 for the radial flow, the effect of block shape is strongest for $l = 5.0$ m and disappears for $l = 0.2$ m, depending on the dimensionless time of the transport time, while the effect of block size is strong for the three cases of l. The effect of thermal dispersion is significant for all of the cases of matrix blocks. By comparison, the fracture temperature front is further retarded in all cases by the heat exchange between the reservoir and the aquitards with large half-thickness, leading to more smeared temperature profiles.

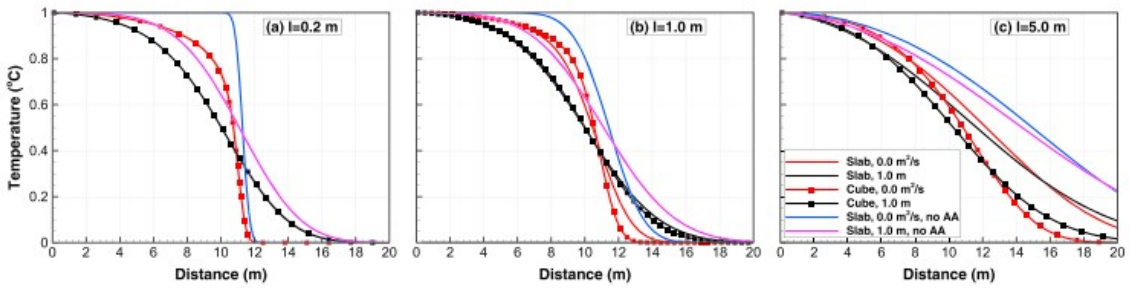

Figure 7. (a–c) Comparison of fracture temperature profiles, as functions effective thermal diffusivity, uniform matrix blocks (slabs and cubes), and minimum fracture half-spacing ($l = 0.2$, 1, and 5), for the radial fluid flow between the fractured reservoir bounded by two aquitards and the fractured reservoir without the A-A coupling (marked by "no AA").

5 Conclusions

Numerous analytical solutions have been developed since the 1950s for modeling temperature perturbations in the subsurface in support of various field applications, such as thermal oil recovery, fluid disposal by deep-well injection, aquifer thermal energy storage, geothermal energy production, and groundwater recharge. Each solution has been presented, with detailed derivation, for a specific boundary value problem, with heat exchange between fractures and matrix blocks and between aquifers and aquitards. The nonoverlapping fracture-matrix and aquifer-aquitard setting is often used with a simplified network with one set of parallel fractures.

In this work, a suite of new analytical solutions $G^*(x,s)$ was developed by plugging a generalized multirate memory function $g^*(s)$ into existing, independent global transfer functions $G_0^*\{x,s\}$ for modeling heat transport in fractured reservoirs with various flow fields. These new solutions in the Laplace domain can be written in the simple form: $G^*(x,s) = B^*(s)G_0^*\{x, s[1+\vartheta g^*(s)]\}$ that also depends on the inlet boundary condition function $B^*(s)$. The multirate memory function was developed for a REV of fractured reservoirs by Laplace transforming the unified-form diffusive flux equation recently developed by Zhou, Oldenburg, Rutqvist, and Birkholzer, (2017) and Zhou, Oldenburg, Spangler, and Birkholzer (2017). The REV was conceptualized to contain well-mixed multiple fractures and multiple matrix blocks of different shapes, sizes, properties, and volume fractions. This conceptualization can easily handle fractured reservoirs with one, two, and three orthogonal sets of discrete fractures with different fracture density and spacing and with resulting matrix blocks (e.g., finite slabs, rectangles, and rectangular parallelepipeds) with different sizes and aspect ratios. The new dual-continuum-based solutions facilitate the consideration of fracture-matrix heat exchange and aquifer-aquitard heat exchange in fractured reservoirs bounded by aquitards using the generalized multirate memory function.

The new solutions were applied to three benchmark problems of heat transport in a single-continuum reservoir, a fractured reservoir, and a fractured reservoir bounded by aquitards. The sensitivity analyses on fluid-flow fields, transport mechanisms, and shape and size of matrix blocks can be summarized as follows: (1) large thermal dispersion ($\alpha_L \geq 1$ m) has a significant effect on smearing temperature fronts in fractures, while the solutions of fracture convection only can be used to accurately approximate solutions with convection-conduction, and convection-conduction-dispersion with $\alpha_L \leq 0.01$ m in fractured reservoirs, (2) the shape and size of matrix blocks significantly affect fracture-matrix heat exchange during the early-time heat exchange regime, while the effect disappears during the fracture-matrix equilibrium regime, depending on the dimensionless times for involved matrix blocks, and (3) thermal retardation is significant in both linear and radial flow, regardless of the heat exchange regimes, due to the high intrinsic thermal diffusivity of the rock matrix.

Acknowledgments

This work was supported by the California Energy Commission (CEC) through an Electric Program Investment Charge (EPIC) funding award on geothermal energy to Lawrence Berkeley National Laboratory (LBNL) under agreement EPC-16-022. This work was also supported by the Assistant Secretary for Fossil Energy, National Energy Technology Laboratory, National Risk Assessment Partnership, U.S. Department of Energy, under award DE-AC02-05CH11231 with LBNL. We note that there are no data-sharing issues

because all of the numerical data shown in the figures are in fact produced by the developed analytical solutions in the paper.

Appendix A: Heat Transport Equations for Different Flow Fields

For 1-D linear fluid and heat flow, q_f and D_{ef} are constant in space and time. Equation 3a can be rewritten as follows:

$$D_{ef}\frac{\partial^2 T_f}{\partial x^2}-\frac{q_f}{R_f}\frac{\partial T_f}{\partial x}-\left[\frac{\partial T_f}{\partial t}+\vartheta\int_0^t g(t')\frac{\partial T_f(t-t')}{\partial t}dt'\right]=0, \quad \text{(A1)}$$

where x is the single space coordinate and q_f is the Darcy's velocity in the x direction. Taking the Laplace transform of equation A1 leads to

$$\frac{\partial^2 T_f^*}{\partial x^2}-\frac{q_f}{R_f D_{ef}}\frac{\partial T_f^*}{\partial x}-\frac{1}{D_{ef}}\left[1+\vartheta g^*(s)\right]sT_f^*=0. \quad \text{(A2)}$$

Equation A2 is a second-order ordinary differential equation for $T_f^*(s)$.

For 1-D radial fluid and heat flow, we have $q_f = Q/(2\pi B_f r) = Q'/r$, where Q is the injection rate, B_f is the reservoir thickness, r is the radial coordinate, and $Q' = Q/2\pi B_f$. In the case of constant $D_{ef} = D_f$ with only intrinsic thermal conduction considered, equation 3a can be rewritten as follows:

$$D_{ef}\frac{\partial^2 T_f}{\partial r^2}+\left[D_{ef}-\frac{Q'}{R_f}\right]\frac{1}{r}\frac{\partial T_f}{\partial r}-\left[\frac{\partial T_f}{\partial t}+\vartheta\int_0^t g(t')\frac{\partial T_f(t-t')}{\partial t}dt'\right]=0. \quad \text{(A3)}$$

Taking the Laplace transform of equation A3 leads to

$$\frac{\partial^2 T_f^*}{\partial r^2}+\left[1-\frac{Q'}{D_{ef}R_f}\right]\frac{1}{r}\frac{\partial T_f^*}{\partial r}-\frac{1}{D_{ef}}\left[1+\vartheta g^*(s)\right]sT_f^*=0. \quad \text{(A4)}$$

Equation A4 can be rewritten, following Avdonin (1964a), Carslaw and Jaeger (1959, p. 389), and Chen and Reddell (1983), in the form

$$\frac{\partial^2 T_f^*}{\partial r^2}+\frac{1}{r}[1-2\nu]\frac{\partial T_f^*}{\partial r}-\frac{1}{D_{ef}}\left[1+\vartheta g^*(s)\right]sT_f^*=0, \quad \text{(A5)}$$

where $\nu = Q/4\pi B_f D_{ef} R_f$.

In the case of dominant dispersion-induced thermal diffusivity in the region with temperature perturbations, $D_{ef} = \alpha_L u_f/R_f = \alpha_L Q'/\phi_f r R_f$. Equation 3a can be rewritten as follows:

$$\frac{\alpha_L}{\phi_f}\frac{Q'}{R_f}\frac{1}{r}\frac{\partial^2 T_f}{\partial r^2}-\frac{Q'}{R_f}\frac{1}{r}\frac{\partial T_f}{\partial r}-\left[\frac{\partial T_f}{\partial t}+\vartheta\int_0^t g(t')\frac{\partial T_f(t-t')}{\partial t}dt'\right]=0. \quad \text{(A6)}$$

Taking the Laplace transform of equation A6 leads to

$$\frac{1}{r}\frac{\partial^2 T_f^*}{\partial r^2}-\frac{\phi_f}{\alpha_L}\frac{1}{r}\frac{\partial T_f^*}{\partial r}-\frac{R_f\phi_f}{Q'\alpha_L}\left[1+\vartheta g^*(s)\right]sT_f^*=0. \quad \text{(A7)}$$

Equation A7 can be further rewritten, with the introduction of dimensionless radius $\varrho = r(\phi_f/\alpha_L)$ (Chen, 1985; Moench & Ogata, 1981; Tang & Babu, 1979), in the form:

$$\frac{1}{\varrho}\frac{\partial^2 T_f^*}{\partial \varrho^2} - \frac{1}{\varrho}\frac{\partial T_f^*}{\partial \varrho} - \frac{R_f \alpha_L^2}{Q' \phi_f^2}\left[1 + \vartheta g^*(s)\right] s T_f^* = 0. \quad \text{(A8)}$$

For 1-D SWIW flow, equations A3 through A8 are applicable to the 1-D diverging fluid and heat flow during the injection period. For the 1-D converging flow during the withdrawal period, we change the sign of the convection, keep the radial coordinate unchanged, and obtain the subsidiary equations for convective-conductive heat transport:

$$\frac{\partial^2 T_f^*}{\partial r^2} + \frac{1}{r}[1 + 2\nu]\frac{\partial T_f^*}{\partial r} - \frac{1}{D_{ef}}\left[1 + \vartheta g^*(s)\right] s T_f^* = -\frac{1}{D_{ef}}\left[T_{f0} + \vartheta \gamma_{m0}^*(s)\right], \quad \text{(A9)}$$

and for convective-dispersive heat transport:

$$\frac{1}{\varrho}\frac{\partial^2 T_f^*}{\partial \varrho^2} + \frac{1}{\varrho}\frac{\partial T_f^*}{\partial \varrho} - \frac{R_f \alpha_L^2}{Q' \phi_f^2}\left[1 + \vartheta g^*(s)\right] s T_f^* = -\frac{R_f \alpha_L^2}{Q' \phi_f^2}\left[T_{f0} + \vartheta \gamma_{m0}^*(s)\right]. \quad \text{(A10)}$$

The right-hand side of equations A9 and A10 is the summation of (1) the contribution from the initial fracture temperature T_{f0} and (2) the contribution from the normalized fracture-matrix heat flux, $\mathcal{L}^{-1}\{\gamma_{m0}^*(s)\}$, induced by the nonuniform initial matrix temperature. The initial temperatures of the fractures and matrix blocks are the solved nonuniform temperatures at the end of the injection period, and the real time starts from the beginning of the withdrawal period. Note that the existing SWIW solutions (Jung & Pruess, 2012; Kocabas, 2005) only account for 1-D linear convection coupled with 1-D conduction in semi-infinite slabs.

For 2-D dipole flow, each streamline between the injection well and the withdrawal well corresponds to a given central angle that varies in the range $[0, \pi]$ from the injection well (Alishaev, 1979; Grove & Beetem, 1971). Equations A1 and A2 may be applicable for the heat transport (with variable longitudinal velocity) along the streamline.

Appendix B: Coefficients for the Diffusive Flux Equation and Memory Function

The parameters in equations 11 and 13a–13f for a slab-like, square-like, cubical, rectangular, and rectangular parallelepiped matrix block can be obtained using the following general equations written for a rectangular parallelepiped with matrix block dimensions $n_d = 3$ (Zhou, Oldenburg, Rutqvist, & Birkholzer, 2017):

$$a_1 = (1 + R_{l2} + R_{l3})/\sqrt{\pi}, \quad \text{(B1)}$$

$$a_2 = -4(R_{l2} + R_{l3} + R_{l2}R_{l3})/\pi, \quad \text{(B2)}$$

$$a_3 = 12R_{l2}R_{l3}/\pi^{3/2}, \quad \text{(B3)}$$

$$b_{1j} = \prod_{i=1}^{n_d} \left(\frac{8}{\pi^2}\right) / \left[(2n_{ij}-1)^2\right], \quad \text{(B4)}$$

$$b_{2j} = \frac{\pi^2}{4} c_j; \quad c_j = \sum_{i=1}^{n_d} (2n_{ij}-1)^2 R_{li}^2, \quad \text{(B5)}$$

where R_{li} (i = 1, 2, 3) are the aspect ratios for the three local coordinates x_i and n_{ij} are the integers in the order 1, 2, 3, … , n_{ij}. The aspect ratios, fracture half-spacing l_i, and dimensionless area-to-volume ratio R are written as follows:

$$R_{li} = l/l_i; l = l_1 \le l_2 \le l_3; \quad R = Al/V, \quad \text{(B6)}$$

where A and V are the surface area and volume of the matrix block. The number of exponential terms (N) is determined practically for anisotropic matrix blocks by

$$c_j < 11-(3-n_d) \text{ with } \quad b_{1j} \exp\left(-b_{2j} t_{d0}\right) \ge \epsilon, \quad \text{(B7)}$$

where is a cutoff that depends on the degree of anisotropy (Zhou, Oldenburg, Spangler, & Birkholzer, 2017). The c_j in equation B7 is used to account for the anisotropy effect while maintaining the first-order approximation in the late-time solution, the same order of approximation as for the early-time solution. N decreases with increased aspect ratios of the matrix block, with N = 1 for an isotropic, cubical matrix block ($l = l_1 = l_2 = l_3$). For a rectangular 2-D matrix block, R_{l3} = 0, and n_d = 2, while for an isotropic slab, $R_{l2} = R_{l3}$ = 0, n_d = 1, and N = 1.

The switchover dimensionless time t_{d0} of 0.22 is used for all shapes of matrix blocks in this study, although there is a slight difference between the optimal values for slabs, spheres, cylinders, squares, cubes, rectangles, and rectangular parallelepipeds; see Table 1 in Zhou, Oldenburg, Spangler, and Birkholzer (2017). As a result, we refit a_2 and a_3 for spheres using the corresponding exact exponential solutions with N = 2,000 and t_{d0} = 0.22, by following the same fitting for cylinders in Zhou, Oldenburg, Spangler, and Birkholzer (2017), and obtain $a_2^s = -3.013$ and $a_3^s = 0.068$ with a relative approximation error less than 0.1%, where superscript s denotes the parameters for spherical matrix blocks. Similarly, we have $a_1^c = 2/\sqrt{\pi}$, $a_2^c = -0.9608$, $a_3^c = -0.5748$, $b_{11}^c = 4/\beta_1^2$, $b_{21}^c = \beta_1^2$, and N = 1 for a cylinder denoted by superscript c.

Appendix C: Laplace Transforms of $\mathcal{L}\left\{U\left(t_d^k - t_{d0}\right) f_e^k\left(t_d^k\right)\right\}$

The following Laplace transform with respect to dimensionless time t_d^k leads to

$$\mathcal{L}_3 = \mathcal{L}\left\{U\left(t_d^k - t_{d0}\right) f_e^k\left(t_d^k\right)\right\} = a_1 \mathcal{L}_4 + a_2 p^{-1} \exp(-p t_{d0}) + a_3 \mathcal{L}_5, \quad \text{(C1)}$$

with

$$\mathcal{L}_4 = \exp(-p t_{d0}) \mathcal{L}\left\{1/\sqrt{t' + t_{d0}}\right\}, \quad \text{(C2)}$$

$$\mathscr{L}_5 = \exp(-pt_{d0})\mathscr{L}\left\{\sqrt{t' + t_{d0}}\right\}, \quad \text{(C3)}$$

Because $\mathscr{L}\left\{1/\sqrt{t' + t_{d0}}\right\}$ is difficult to derive, we use the exact Laplace transform of the dimensionless diffusive flux for a slab-like matrix block written in terms of dimensionless time t_d^k (Dentz & Berkowitz, 2003; Haggerty et al., 2000; Villermaux, 1987; Zhou et al., 2009):

$$\mathscr{L}\{f_d^k\} = \frac{\tanh\sqrt{p}}{\sqrt{p}} \quad \text{(C4)}$$

to match the Laplace transform in equations B1–B6 for a slab with $a_1 = 1/\sqrt{\pi}$, $a_2 = a_3 = 0$, $b_{11} = 8/\pi^2$, $b_{21} = \pi^2/4$, and $N = 1$ and obtain

$$\mathscr{L}_4 = \sqrt{\pi}\left\{\frac{1-\tanh\sqrt{p}}{\sqrt{p}} + \frac{2\exp[-(p+\pi^2/4)t_{d0}]}{p+\pi^2/4}\right\}. \quad \text{(C5)}$$

Because $\mathscr{L}\left\{\sqrt{t' + t_{d0}}\right\}$ is also difficult to derive, we use the exact Laplace transform of the dimensionless diffusive flux for a spherical matrix block (Dentz & Berkowitz, 2003; Haggerty et al., 2000; Moench, 1995; Villermaux, 1987):

$$\mathscr{L}\{f_d^k\} = \frac{3}{\sqrt{p}}\left(\coth\sqrt{p} - \frac{1}{\sqrt{p}}\right) \quad \text{(C6)}$$

to match equations B1–B6 for a sphere with $a_1 = 3/\sqrt{\pi}$, $a_2 = -3.013$, $a_3 = 0.068$, $b_{11} = 6/\pi^2$, $b_{21} = \pi^2$, and $N = 1$ and obtain

$$\mathscr{L}_5 = \frac{1}{a_3^s}\left\{\left[\mathscr{L}_1^s + \frac{6\exp[-(p+\pi^2)t_{d0}]}{p+\pi^2} - \frac{3}{\sqrt{p}}\left(\coth\sqrt{p} - \frac{1}{\sqrt{p}}\right)\right] - a_1^s\mathscr{L}_4 - a_2^s p^{-1}\exp(-pt_{d0})\right\}. \quad \text{(C7)}$$

Alternatively, we can use the exact Laplace transform of the dimensionless diffusive flux for a cylindrical matrix block (Haggerty et al., 2000; Villermaux, 1987):

$$\mathscr{L}\{f_d^k\} = \frac{2}{\sqrt{p}}\frac{I_0(\sqrt{p})}{I_1(\sqrt{p})} \quad \text{(C8)}$$

to match equations B1–B6 for a cylinder with $a_1 = 2/\sqrt{\pi}$, $a_2 = -0.9608$, $a_3 = -0.5748$, $b_{11} = 4/\beta_1^2$, $b_{21} = \beta_1^2$, and $N = 1$ and obtain

$$\mathscr{L}_5 = \frac{1}{a_3^c}\left\{\left[\mathscr{L}_1^c + \frac{4\exp\left[-(p+\beta_1^2)t_{d0}\right]}{p+\beta_1^2} - \frac{2}{\sqrt{p}}\frac{I_0(\sqrt{p})}{I_1(\sqrt{p})}\right] - a_1^c\mathscr{L}_4 - a_2^c p^{-1}\exp(-pt_{d0})\right\}. \quad \text{(C9)}$$

Note that equation 13e is the same as equation C5 and equation 13f is the same as equation C9. $\mathscr{L}_1^s$ and $\mathscr{L}_1^c$ can be referred to equation 13b for spheres and cylinders.

References

Abbasi, M., Khazali, N., & Sharifi, M. (2017). Analytical model for convection-conduction heat transfer during water injection in fractured geothermal reservoirs with variable rock matrix block size. *Geothermics*, 69, 1– 14. https://doi.org/10.1016/j.geothermics.2017.04.002

Abramowitz, M., & Stegun, I. A. (1972). *Handbook of mathematical functions with formulas, graphs, and mathematical tables*. New York, NY: Dover Publications, Inc.

Alishaev, M. G. (1979). Calculation of the temperature field of a porous stratum when fluid is injected for plane flow. *Fluid Dynamics*, 14(1), 49– 56. https://doi.org/10.1007/BF01050812

Andersson, O., Ekkestubbe, J., & Ekdahl, A. (2013). UTES (underground thermal energy storage)—Applications and market development in Sweden. *Journal of Energy and Power Engineering*, 7, 669– 678.

Ascencio, F., Samaniego, F., & Rivera, J. (2014). A heat loss analytical model for the thermal front displacement in naturally fractured reservoirs. *Geothermics*, 50, 112– 121. https://doi.org/10.1016/j.geothermics.2013.09.002

Avdonin, N. A. (1964a). Some formulas for calculating the temperature field of a stratum subject to thermal injection. *Neft'i Gaz*, 7(3), 37.

Avdonin, N. A. (1964b). On the different methods of calculating the temperature fields of a stratum during thermal injection. *Neft'i Gaz*, 7(8), 39.

Barenblatt, G. E., Zheltov, I. P., & Kochina, I. N. (1960). Basic concepts in the theory of homogeneous liquids in fissured rocks. *Journal of Applied Mathematics and Mechanics*, 24(5), 1286– 1303. https://doi.org/10.1016/0021-8928(60)90107-6

Bear, J. (1972). *Dynamics of fluids in porous media*. New York, NY: Dover Publications Inc.

Bodvarsson, G. (1969). On the temperature of water flowing through fractures. *Journal of Geophysical Research*, 74(8), 1987– 1992. https://doi.org/10.1029/JB074i008p01987

Bodvarsson, G., & Eggers, D. E. (1972). The energy of thermal water. *Geothermics*, 1(3), 93– 95. https://doi.org/10.1016/0375-6505(72)90033-8

Bodvarsson, G. S., & Tsang, C.-F. (1982). Injection and thermal breakthrough in fractured geothermal reservoirs. *Journal of Geophysical Research*, 87(B2), 1031– 1048. https://doi.org/10.1029/JB087iB02p01031

Bredehoeft, J. D., & Papadopulos, I. S. (1965). Rates of vertical groundwater movement estimated from the Earth's thermal profile. *Water Resources Research*, 1(2), 325– 328. https://doi.org/10.1029/WR001i002p00325

Carrera, J., Sanchez-Vila, X., Benet, I., Medina, A., Galarza, G., & Guimera, J. (1998). On matrix diffusion: Formulations, solution methods and qualitative effects. *Hydrogeology Journal*, 6(1), 178– 190. https://doi.org/10.1007/s100400050143

Carslaw, H. S., & Jaeger, J. C. (1959). *Conduction of heat in solids* (2nd ed.). Oxford, UK: Clarendon.

Chen, C.-S. (1985). Analytical and approximate solutions to radial dispersion from an injection well to a geological unit with simultaneous diffusion into adjacent strata. *Water Resources Research*, 21(8), 1069– 1076. https://doi.org/10.1029/WR021i008p01069

Chen, C.-S., & Reddell, D. L. (1983). Temperature distribution around a well during thermal injection and a graphical technique for evaluating aquifer thermal properties. *Water Resources Research*, 19(2), 351– 363. https://doi.org/10.1029/WR019i002p00351

Constantz, J., Stewart, A. E., Niswonger, R., & Sarma, L. (2002). Analysis of temperature profiles for investigating stream losses beneath ephemeral channels. *Water Resources Research*, 38(12), 1316. https://doi.org/10.1029/2001WR001221

Danckwerts, P. V. (1953). Continuous flow systems: Distribution of residence times. *Chemical Engineering Science*, 2(1), 1– 13. https://doi.org/10.1016/0009-2509(53)80001-1

de Hoog, F. R., Knight, J. H., & Stokes, A. N. (1982). An improved method for numerical inversion of Laplace transforms. *SIAM Journal on Scientific and Statistical Computing*, 3(3), 357– 366. https://doi.org/10.1137/0903022

Dentz, M., & Berkowitz, B. (2003). Transport behavior of a passive solute in continuous time random walks and multirate mass transfer. *Water Resources Research*, 39(5), 1111. https://doi.org/10.1029/2001WR001163

Detwiler, R. L., Rajaram, H., & Glass, R. J. (2000). Solute transport in variable–aperture fractures: An investigation of the relative importance of Taylor dispersion and macrodispersion. *Water Resources Research*, 36(7), 1611– 1625. https://doi.org/10.1029/2000WR900036

Green, D. W., Perry, R. H., & Babcock, R. E. (1964). Longitudinal dispersion of thermal energy through porous media with a flowing fluid. *AICHE Journal*, 10(5), 645– 651. https://doi.org/10.1002/aic.690100514

Gringarten, A., & Sauty, J. (1975). A theoretical study of heat extraction from aquifers with uniform regional flow. *Journal of Geophysical Research*, 80(35), 4956– 4962. https://doi.org/10.1029/JB080i035p04956

Gringarten, A., Witherspoon, P., & Ohnishi, Y. (1975). Theory of heat extraction from fractured hot dry rock. *Journal of Geophysical Research*, 80(8), 1120– 1124. https://doi.org/10.1029/JB080i008p01120

Grove, D. B., & Beetem, W. A. (1971). Porosity and dispersion constant calculations for a fractured carbonate aquifer using the two-well tracer method. *Water Resources Research*, 7(1), 128– 134. https://doi.org/10.1029/WR007i001p00128

Guan, J., Molz, F. J., Zhou, Q., Liu, H.-H., & Zheng, C. (2008). Behavior of the mass transfer coefficient during the MADE-2 experiment: New insights. *Water Resources Research*, 44, W02423. https://doi.org/10.1029/2007WR006120

Haggerty, R., McKenna, S. A., & Meigs, L. C. (2000). On the late-time behavior of tracer test breakthrough curves. *Water Resources Research*, 36(12), 3467– 3479. https://doi.org/10.1029/2000WR900214

Harlow, F. H., & Pracht, W. E. (1972). A theoretical study of geothermal energy extraction. *Journal of Geophysical Research*, 77(35), 7038– 7048. https://doi.org/10.1029/JB077i035p07038

Hatch, C. E., Fisher, A. T., Revenaugh, J. S., Constantz, J., & Ruehl, C. (2006). Quantifying surface water–groundwater interactions using time series analysis of streambed thermal records: Method development. *Water Resources Research*, 42, W10410. https://doi.org/10.1029/2005WR004787

Hawkins, A. J., Becker, M. W., & Tsoflias, G. P. (2017). Evaluation of inert tracers in a bedrock fracture using ground penetrating radar and thermal sensors. *Geothermics*, 67, 86– 94. https://doi.org/10.1016/j.geothermics.2017.01.006

Hyman, J. D., Karra, S., Makedonska, N., Gable, C. W., Painter, S. L., & Viswanathan, H. S. (2015). dfnWorks: A discrete fracture network framework for modeling subsurface flow and transport. *Computers & Geosciences*, 84, 10– 19. https://doi.org/10.1016/j.cageo.2015.08.001

Jung, Y., & Pruess, K. (2012). A closed-form analytical solution for thermal single-well injection-withdrawal tests. *Water Resources Research*, 48, W03504. https://doi.org/10.1029/2011WR010979

Kocabas, I. (2004). Thermal transients during nonisothermal fluid injection into oil reservoirs. *Journal of Petroleum Science and Engineering*, 42(2-4), 133– 144. https://doi.org/10.1016/j.petrol.2003.12.006

Kocabas, I. (2005). Geothermal reservoir characterization via thermal injection-backflow and interwell tracer testing. *Geothermics*, 34(1), 27– 46. https://doi.org/10.1016/j.geothermics.2004.09.003

Kreft, A., & Zuber, A. (1978). On the physical meaning of the dispersion equation and its solutions for different initial and boundary conditions. *Chemical Engineering Science*, 33(11), 1471– 1480. https://doi.org/10.1016/0009-2509(78)85196-3

Kuhn, C. S., & Koch, R. L. (1953). In situ combustion newest method of increasing oil recovery. *Oil and Gas Journal*, 52(14), 92.

Kuwahara, F., & Nakayama, A. (1999). Numerical determination of thermal dispersion coefficients using a periodic structure. *ASME Journal of Heat Transfer*, 121(1), 160– 163. https://doi.org/10.1115/1.2825930

Lauwerier, H. A. (1955). The transport of heat in an oil layer caused by the injection of hot fluid. *Applied Scientific Research, Section A*, 5(2–3), 145– 150. https://doi.org/10.1007/BF03184614

Li, K.-Y., Yang, S.-Y., & Yeh, H.-D. (2010). An analytical solution for describing the transient temperature distribution in an aquifer thermal energy storage system. *Hydrological Processes*, 24(25), 3676– 3688. https://doi.org/10.1002/hyp.7779

Lim, K. T., & Aziz, K. (1995). Matrix-fracture transfer shape factors for dual-porosity simulators. *Journal of Petroleum Science and Engineering*, 13(3-4), 169– 178. https://doi.org/10.1016/0920-4105(95)00010-F

Malofeev, G. E. (1960). Calculation of the temperature distribution in a formation when pumping hot fluid into a well. *Nefti Gaz*, 3(7), 59.

Metzger, T., Didierjean, S., & Maillet, D. (2004). Optimal experimental estimation of thermal dispersion coefficients in porous media. *International Journal of Heat and Mass Transfer*, 47(14-16), 3341– 3353. https://doi.org/10.1016/j.ijheatmasstransfer.2004.02.024

Meyer, C. F., & Todd, D. K. (1973). Heat storage wells. *Water Well Journal*, 27, 35– 41.

Moench, A. F. (1984). Double-porosity models for a fissured groundwater reservoir with fracture skin. *Water Resources Research*, 20(7), 831– 846. https://doi.org/10.1029/WR020i007p00831

Moench, A. F. (1995). Convergent radial dispersion in a double-porosity aquifer with fracture skin: Analytical solution and application to a field experiment in fractured chalk. *Water Resources Research*, 31(8), 1823– 1835. https://doi.org/10.1029/95WR01275

Moench, A. F., & Ogata, A. (1981). A numerical inversion of the Laplace transform solution to radial dispersion in a porous medium. *Water Resources Research*, 17(1), 250– 252. https://doi.org/10.1029/WR017i001p00250

Molina-Giraldo, N., Bayer, P., & Blum, P. (2011). Evaluating the influence of thermal dispersion on temperature plumes from geothermal systems using analytical solutions. *International Journal of Thermal Sciences*, 50(7), 1223– 1231. https://doi.org/10.1016/j.ijthermalsci.2011.02.004

Neretnieks, I. (1980). Diffusion in the rock matrix: An important factor in radionuclide retardation? *Journal of Geophysical Research*, 85(B8), 4379– 4397. https://doi.org/10.1029/JB085iB08p04379

Nordbotten, J. M. (2017). Analytical solutions for aquifer thermal energy storage. *Water Resources Research*, 53, 1354– 1368. https://doi.org/10.1002/2016WR019524

Noyer, M. L. (1977). *Simulation des transferts thermiques dans les aquifers: Conditions de validite des solutions analytiques*. Rap-BRGM 77 SGN (Vol. 598, p. 33). Orléans, France: HYD, BRGM.

Ogata, A., & Banks, R. B. (1961). A solution of the differential equation of longitudinal dispersion in porous media. Geological Survey Professional Paper 411-A. United States Geological Survey.

Ozgumus, T., Mobedi, M., Ozkol, U., & Nakayama, A. (2013). Thermal dispersion in porous media—A review on the experimental studies for packed beds. *Applied Mechanics Reviews*, 65(3), 031001. https://doi.org/10.1115/1.4024351

Park, Y.-J., de Dreuzy, J.-R., Lee, K.-K., & Berkowitz, B. (2001). Transport and intersection mixing in random fracture networks with power law length distributions. *Water Resources Research*, 37(10), 2493– 2501. https://doi.org/10.1029/2000WR000131

Pruess, K., & Narasimhan, T. N. (1985). A practical method for modeling fluid and heat flow in fractured porous media. *Society of Petroleum Engineers Journal*, 25(01), 14– 26. https://doi.org/10.2118/10509-PA

Rau, G. C., Andersen, M. S., & Acworth, R. I. (2012). Experimental investigation of the thermal dispersivity term and its significance in the heat transport equation for flow in sediments. *Water Resources Research*, 48, W03511. https://doi.org/10.1029/2011WR011038

Reimus, P., Pohll, G., Mihevc, T., Chapman, J., Haga, M., Lyles, B., Kosinski, S., Niswonger, R., & Sanders, P. (2003). Testing and parameterizing a conceptual model for solute transport in a fractured granite using multiple tracers in a forced-gradient test. *Water Resources Research*, 39(12), 1356. https://doi.org/10.1029/2002WR001597

Rubinshtein, L. I. (1960). A contact thermal conduction problem. *Dan SSSR*, 135(4), 805 B05.

Rubinshtein, L. I. (1962). An asymptotic solution of an axially symmetric contact problem in thermal convection for high values of the convection parameter. *Dan SSSR*, 146(5), 1043.

Ruiz Martínez, Á., Roubinet, D., & Tartakovsky, D. M. (2014). Analytical models of heat conduction in fractured rocks. *Journal of Geophysical Research: Solid Earth*, 119, 83– 98. https://doi.org/10.1002/2012JB010016

Saada, M. A., Chikh, S., & Campo, A. (2006). Analysis of hydrodynamic and thermal dispersion in porous media by means of a local approach. *Heat and Mass Transfer*, 42(11), 995– 1006. https://doi.org/10.1007/s00231-005-0061-y

Sandve, T. H., Berre, I., & Nordbotten, J. M. (2012). An efficient multi-point flux approximation method for discrete fracture–matrix simulations. *Journal of Computational Physics*, 231(9), 3784– 3800. https://doi.org/10.1016/j.jcp.2012.01.023

Sardin, M., Schweich, M., Leij, F. J., & van Genuchten, M. T. (1991). Modeling the nonequilibrium transport of linearly interacting solutes in porous media: A review. *Water Resources Research*, 27(9), 2287– 2307. https://doi.org/10.1029/91WR01034

Sauty, J. P., Gringarten, A. C., Menjoz, A., & Landel, P. A. (1982). Sensible energy storage in aquifer: Theoretical study. *Water Resources Research*, 18(2), 245– 252. https://doi.org/10.1029/WR018i002p00245

Silliman, S. E., Ramirez, J., & McCabe, R. L. (1995). Quantifying downflow through creek sediments using temperature time series: One-dimensional solution incorporating measured surface temperature. *Journal of Hydrology*, 167(1–4), 99– 119. https://doi.org/10.1016/0022-1694(94)02613-G

Spillette, A. (1965). Heat transfer during hot fluid injection into an oil reservoir. *Journal of Canadian Petroleum Technology*, 4(04), 213– 218. https://doi.org/10.2118/65-04-06

Stallman, R. W. (1965). Steady one-dimensional fluid flow in a semi-infinite porous medium with sinusoidal surface temperature. *Journal of Geophysical Research*, 70(12), 2821– 2827. https://doi.org/10.1029/JZ070i012p02821

Sudicky, E. A., & Frind, E. O. (1982). Contaminant transport in fractured porous media: Analytical solutions for a system of parallel fractures. *Water Resources Research*, 18(6), 1634– 1642. https://doi.org/10.1029/WR018i006p01634

Suzuki, S. (1960). Percolation measurements based on heat flow through soil with special reference to paddy fields. *Journal of Geophysical Research*, 65(9), 2883– 2885. https://doi.org/10.1029/JZ065i009p02883

Tang, D. H., & Babu, D. K. (1979). Analytical solution of a velocity dependent dispersion problem. *Water Resources Research*, 15(6), 1471– 1478. https://doi.org/10.1029/WR015i006p01471

Tang, D. H., Frind, E. O., & Sudicky, E. A. (1981). Contaminant transport in fractured porous media: Analytical solution for a single fracture. *Water Resources Research*, 17(3), 555– 564. https://doi.org/10.1029/WR017i003p00555

Tsang, C.-F., Hopkins, D., & Hellstrom, G. (1982). Aquifer thermal energy storage: A survey. Special Paper 189 (pp. 427– 441). American: Geological Society. https://doi.org/10.1130/SPE189-p427

Vafai, K., & Tien, C. L. (1981). Boundary and inertia effects on flow and heat transfer in porous media. *International Journal of Heat and Mass Transfer*, 24(2), 195– 203. https://doi.org/10.1016/0017-9310(81)90027-2

Villermaux, J. (1987). Chemical engineering approach to dynamic modeling of linear chromatography: A flexible method for representing complex phenomena from simple concepts. *Journal of Chromatography*, 406, 11– 26. https://doi.org/10.1016/S0021-9673(00)94014-7

Walter, H. (1957). Application of heat for recovery of oil: Field test results and possibility of profitable operation. *Journal of Petroleum Technology*, 9(2), 16.

Warren, J. P., & Root, P. J. (1963). The behavior of naturally fractured reservoirs. *Society of Petroleum Engineers Journal*, 3(03), 245– 255. https://doi.org/10.2118/426-PA

Yagi, S., Kunii, D., & Wakao, N. (1960). Studies on axial effective thermal conductivities in packed beds. *AICHE Journal*, 6(4), 543– 546. https://doi.org/10.1002/aic.690060407

Yang, S.-Y., & Yeh, H.-D. (2009). Modeling heat extraction from hot dry rock in a multi-well system. *Applied Thermal Engineering*, 29(8-9), 1676– 1681. https://doi.org/10.1016/j.applthermaleng.2008.07.020

Zhou, Q., Birkholzer, J. T., & Tsang, C.-F. (2009). A semi-analytical solution for large-scale injection-induced pressure perturbation and leakage in a laterally bounded aquifer-aquitard system. *Transport in Porous Media*, 78(1), 127– 148. https://doi.org/10.1007/s11242-008-9290-0

Zhou, Q., Liu, H.-H., Bodvarsson, G. S., & Molz, F. J. (2006). Evidence of multi-process matrix diffusion in a single fracture from a field tracer test. *Transport in Porous Media*, 63(3), 473– 487. https://doi.org/10.1007/s11242-005-1123-9

Zhou, Q., Liu, H.-H., Molz, F. J., Zhang, Y., & Bodvarsson, G. S. (2007). Field-scale effective matrix diffusion coefficient for fractured rock: Results from literature survey. *Journal of Contaminant Hydrology*, 93(1-4), 161– 187. https://doi.org/10.1016/j.jconhyd.2007.02.002

Zhou, Q., Oldenburg, C. M., Rutqvist, J., & Birkholzer, J. T. (2017). Revisiting the fundamental analytical solutions of heat and mass transfer: The kernel of multirate and multidimensional diffusion. *Water Resources Research*, 53, 9960– 9979. https://doi.org/10.1002/2017WR021040

Zhou, Q., Oldenburg, C. M., Spangler, L. H., & Birkholzer, J. T. (2017). Approximate solutions for diffusive fracture-matrix transfer: Application to storage of dissolved CO_2 in fractured rocks. *Water Resources Research*, 53, 1746– 1762. https://doi.org/10.1002/2016WR019868